Supplementary Information

Reconciling the total carbon budget for boreal forest wildfire emissions using airborne observations

Katherine L. Hayden[1]*, Shao-Meng Li[2], John Liggio[1], Michael J. Wheeler[1], Jeremy J.B. Wentzell[1], Amy Leithead[1], Peter Brickell[1], Richard L. Mittermeier[1], Zachary Oldham[1,6], Cris Mihele[1], Ralf M. Staebler[1], Samar G. Moussa[1], Andrea Darlington[1], Alexandra Steffen[1], Mengistu Wolde[3], Daniel Thompson[4], Jack Chen[1], Debora Griffin[1], Ellen Eckert[1], Jenna C. Ditto[5], Megan He[5] and Drew R. Gentner[5]

[1]{Air Quality Research Division, Environment Canada, Toronto, ON, Canada}
[2]{College of Environmental Sciences and Engineering, Peking University, Beijing, China}
[3]{National Research Council of Canada, Ottawa, ON, Canada}
[4]{Canadian Forest Service, Natural Resources Canada, Edmonton, ON, Canada}
[5]{Yale University, New Haven, CT, USA}
[6]{University of Waterloo, Waterloo, ON, Canada}

*Correspondence to: Katherine Hayden (katherine.hayden@ec.gc.ca)

2.0 Methods

2.1 Aircraft measurements

Table S1 provides a summary of the measurements with associated instrumentation, technical details and related references.

2.1.1 Trace gas measurements

All of the trace gas instrumentation except NH_3 and the CIMS were sampled through PTFE tubing from a main aircraft roof hatch that contained multiple inlet ports through which rear-facing tubing was mounted.

NO, NO_2, NO_y, SO_2 and GEM These measurements were made using modified commercial instruments (Thermo Scientific Inc. and Tekran Instruments Corp.). NO and SO_2 were directly measured: NO by chemiluminescence with excess ozone using a 42i TL instrument operated in single mode, while SO_2 was

measured by pulsed fluorescence with a 43i TL instrument. A photolytic converter (Air Quality Design Inc.) was used to selectively convert a large fraction of NO_2 to NO. The sum of this NO_2 fraction that was converted to NO plus ambient NO, defined as NO_c, was measured by a second 42i TL chemiluminescent instrument and then NO_2 was calculated based on NO_c, NO and the efficiency of the photolytic converter. NO_y was measured by using an external molybdenum converter heated at 325 °C and placed as close as possible to the sampling point, followed by a third 42i TL instrument. NO and SO_2 calibrations were conducted by generating mixing ratios of 0-100 ppbv using NIST certified cylinders from Scott-Marin (10.3 ppmv accuracy: +/- 2 %), an Environics (Model 6100 Multi-Gas Calibrator), and a Sabio Zero Generator (Model 1001). The efficiencies of the photolytic and NO_y converters were determined using the gas phase titration option of the Environics calibrator. Gas phase elemental Hg (GEM) was measured with a Tekran 237X instrument (Tekran Instruments Corporation) modified to allow a reduced sampling time of 2 min (McLagan et al., 2021; Cole et al., 2014).

NH_3 Ammonia (NH_3) measurements were conducted using Los Gatos Research's (LGR's) NH_3/H_2S Analyzer (Model 911-0039) sampled through an unfiltered inlet, critical orifice and 4 m of 6.35 mm (¼") outer diameter Sulfinert-coated tubing heated to 90 °C to minimize NH_3 losses to the tubing walls. The flow rate was 2.5 LPM, controlled through a critical orifice near the unfiltered inlet with the pressure in the fluoropel-coated LGR cell being maintained at 100 Torr. For instrument zeros, ambient air was passed through a Teflon filter coated with citric acid. Calibrations were performed using a certified ammonia standard (Air Liquide; 10.0 ppm NH_3 in N_2, accuracy: +/- 5 %), diluted to near-ambient levels.

CO, CO_2, CH_4, TC and $NMOG_T$ CO, CO_2, CH_4 were measured with a Cavity Ring Down (CRD) spectroscopy instrument (Picarro G2401-m). A second Picarro G2401-m instrument was used to measure total carbon (TC, in units of ppmC) by passing the sample air through a heated (650 °C) platinum catalyst (Shimadzu), adapted from Stockwell et al. (2018) and Veres et al., (2010). $NMOG_T$ mixing ratios in units of ppmC was quantified by subtracting the ambient CH_4, CO and CO_2 measurements (instrument without the upstream catalyst) from the TC measurements.

Calibrations using two different mixing ratio standards of CO, CO_2 and CH_4 were performed for both instruments at the beginning and end of each flight to assess instrument drift and sensitivity. $NMOG_T$ was averaged to 10 sec (from the 2 sec native time resolution) to increase the signal to noise. Laboratory experiments indicated that the conversion efficiency of ethane across the catalyst was ~100 %, which is expected to be the most challenging species to combust aside from methane, which is concurrently measured. Additional laboratory experiments using a range of hydrocarbons ($>C_2$) including aromatics also exhibited ~100 % conversion efficiency (Li et al., 2021; Li et al., 2019). The catalyst material was changed after approximately every 5 flights to further ensure minimal changes in efficiency.

CIMS The CIMS (modified Tofwerk/Aerodyne Api-ToF) instrument sampled from an insulated rear-facing inlet (PFA, 3/8" OD, ¼" ID) at 7 LPM (0°C, 1 atm). The instrument was operated using iodide as a reagent ion. The mass resolution at an internal standard peak ($^{13}CC_2H_6O_2I$-) was ~5400 Th/Th. The reagent ion was generated by passing 2 sLpm (0°C, 1 atm) of UHP N_2 over a methyl iodide permeation tube held at 40 °C. This flow was then passed through a Polonium-210 ionizer (NRD P-2031) into the ion molecule reactor (IMR). A flow of humidified N_2 (20 sccm through a stainless steel bubbler) was also added to the IMR in order to keep the ratio of $I(H_2O)^-/I^-$ as constant as possible. The IMR and small segmented quadrupoles (SSQ) were pressure controlled to 70 and 1.5 mBar respectively using Alicat pressure controllers (PC-EXTSEN). Instrument zeros were performed every 15 min by flooding the inlet with 10 sLpm (0°C, 1 atm) of air that had been passed through a Pt/Pd catalyst (CD Nova) heated to 350 °C followed by bicarbonate and charcoal scrubbers (United Filtration). A flow (50 sccm) of isotopically labelled propanoic acid ($^{13}CC_2H_6O_2$) was constantly added to the inlet during the campaign to track instrument sensitivity. Compounds were identified using known/expected sensitivities and available calibration standards (Tables S3).

PTRMS The PTR-ToF-MS (Ionicon Analytik GmbH, Austria) used chemical ionization with H_3O^+ as the primary reagent ion in a configuration described previously (Table S1). Gases with a proton affinity

greater than that of water were protonated in the drift tube. The pressure and temperature of the drift tube region were maintained at a constant 2.15 mbar and 60 °C, respectively for an E/N of 141 Td. The unit contained a catalytic converter heated to 350 °C with a continuous flow of ambient air at a flow rate of one litre per minute. A permeation tube with 1,2,4-trichlorbenzene was placed at the inlet to improve the sensitivity of the mass calibration for higher masses. Instrumental backgrounds were performed in flight using a custom-built zero-air generating unit. The data were processed using Tofware software (Tofwerk AG). Calibrations were performed on the ground using gas standard mixtures from Ionicon, Apel-Reimer and Scott-Marrin for 20 compounds (Table S3). For compounds with no available gas standard, a relative response factor was calculated with reaction rate constants using the method described in Sekimoto et al. (2017) and guided by the work of Koss et al. (2018) to define an additional 169 ions. Compound identifications for molecular formulas for the PTRMS and CIMS data were assigned based on a limited set of possibilities (particularly for the smaller compounds), known or expected compound sensitivities, and previously published laboratory work by Koss et al. (2018); this is more fully described in the SI Sect. 2.1.3.

AWAS The Advanced Whole Air Sampler (AWAS) was used to take 20-30 sec integrated 'grab' samples using 1.33-litre electropolished stainless steel canisters in rack-mounted arrays of 12-canister modules (Lerner et al., 2017, and references therein). A metal bellows compressor (Senior Aerospace Metal Bellows, MB-158) was used to pressurize canisters to approximately 30 PSI over a period of approximately 15 sec (30 sec maximum). Sample lines and manifold tubing were continually flushed with ambient air during the flights. Sampling took place by activating module and pump system valving with custom Labview-based software operating a data logger interface (Labjack Corp., Model T7). The samples were analysed and cleaned as soon as possible after the flight with an analytical system installed at the Fort McMurray International Airport. The on-site analytical system consisted of a custom fabricated gas chromatograph (GC) system using cryogenic sample pre-concentration, 2-dimensional gas chromatography, Mass Spectrometric Detection (MS) and Flame Ionization Detection (FID). Sample air was cryogenically trapped at -185 °C on a glass bead-filled trap, thus condensing/solidifying the

hydrocarbons, and subsequently thermally desorbing them at 135 °C into the multi-column, multi-oven GC/MS/FID instrument. Trapped sample air volumes were calculated by recording pressure differences in a volume-calibrated downstream vacuum vessel before and after sample trapping. Duplicate analysis was carried out on one canister in each AWAS module. The analytical separation of approximately 120 chemical species was carried out by use of a pre-column (SPB-1) where the initial separation of compounds according to boiling point occurred. The low molecular weight compounds (C_2 to C_4) were then directed to two RTX-QS columns connected in series and quantified by a FID. The higher molecular weight compound stream (C_4 to C_{10}) was subsequently split and simultaneously analysed by a second FID connected to an Aluminum Oxide/KCL column (C_4 to C_8) and by a quadrupole Mass Spectrometer (Agilent Technologies, 5977B) connected to an HP-1 column by means of a fused silica tubing restrictor (C_7 to C_{10}). The precolumn and RTX-QS columns were mounted in the main oven of the gas chromatograph (Agilent Technologies 7890B) and thus were subject to one temperature program. The AlOx/KCL and HP-1 analytical columns were each mounted in a separate temperature-controlled GC oven module (Agilent Technologies, LTM Series II) and operated with a different temperature program. Detector peak areas were calibrated with primary gas standard mixtures in the ppbv concentration range obtained from Apel-Reimer Environmental Inc. (U.S.A.) and the National Physical Laboratory (UK). Compound retention time drift and potential detector sensitivity changes were monitored and compensated for by means of daily analysis of a secondary standard gas. The AWAS modules were cleaned by a custom-fabricated, automated cleaning system similar to that of Lerner et al. (2017).

Cartridges Integrated gas phase samples were collected using an automated adsorbent tube sampling assembly (i.e. cartridge) that was mounted in an under-wing pod (see Ditto et al., 2021; SI Sect. 2.1.1). Samples were collected over the lower set of aircraft transects and higher set of transects, resulting in two integrated cartridge samples for each screen; only the lower altitude samples are used in the analysis as the samples for the higher set of transects included a transect that was above the wildfire plume. Samples were shipped to Yale University where offline analysis was conducted using thermal desorption (GERSTEL TD 3.5+) followed by gas chromatography (Agilent 7890B), atmospheric pressure chemical

ionization, and high-resolution mass spectrometry (Agilent 6550) to speciate gas-phase organic compounds (Ditto et al., 2021, Sheu et al., 2018, Khare et al., 2019). The samples provided targeted measurements of gas-phase compounds ranging in volatility from C_{10} volatile organic compounds (VOCs) to C_{25} semivolatile organic compounds (SVOCs) including hydrocarbons (CH) as well as functionalized compounds containing 1 oxygen atom (CHO_1), and 1 sulfur atom (CHS_1). Ion abundances were converted to mass concentrations assuming average response factors that were calculated based on calibrations using the NIST Reference Gulf of Mexico 2779 Macondo Crude oil reference material following Khare et al. (2019), which accounts for variations in response and fragmentation between components of the complex mixture. We acknowledge the limited sample numbers based on flight design, and that the reported emissions are subject to potential variations in sampling efficiency within the under-wing sampling pod across C_{10}-C_{25} and, in the event of losses, would likely be considered lower limit estimates. CHN_1 was not quantitatively converted to mass due to the lack of available standards. For CH, CHO_1, and CHS_1, each group of isomers at a given carbon number was categorized by molecular formula, according to their double bond equivalents (DBE) ranging from 0 to 15. Emission ratios (to in-plume CO) were estimated for CH, CHO_1 and CHS_1 using observed concentrations for the C_{10}-C_{25} species summed across DBEs. Further discussion of these methods can be found in Ditto et al. (2021), including in the SI (i.e., Section S3).

2.1.2 Particle measurements

Particles were sampled from a forward-facing isokinetic stainless steel diffuser inlet (Droplet Measurement Technologies) that was positioned near the top of the fuselage forward of the engine on the starboard side. Theoretical calculations that take into account the inlet dimensions, volume flow and velocity indicated a 97 % transmission efficiency for particles < 1 μm through the inlet. Air was pulled through the inlet into a main 0.5" O.D. stainless steel sampling line maintained at the isokinetic rate of 70 LPM by two venturis mounted on the fuselage in the aft section of the aircraft. The aerosol instruments subsampled from the main sampling line.

AMS The high resolution aerosol mass spectrometer (AMS) (Aerodyne) measures submicron particles that are sampled through a critical orifice and focussed through an aerodynamic lens into a region of low vacuum. The particles impact a heated surface (600 °C), are vapourized and ionized by 70eV impaction. Ions are then transferred to a time-of-flight mass spectrometer (Tofwerk) where they are accelerated by electric fields and separated by their velocities which are dependent on their mass to charge ratios. Ions are then detected by charged microchannel plates. The AMS was operated only in V mode with 10 sec time resolution. Several ionization efficiency calibrations performed prior to and during the field campaign varied by <10 %. To determine the AMS collection efficiency, number concentrations measured by an Ultra High Sensitivity Aerosol Spectrometer (UHSAS; Droplet Measurement Technologies Inc.) over a size range of 60 nm to 1 µm were converted to volume concentrations using mid-point bin diameters and assuming spherical shapes. Volume concentrations were converted to mass concentrations using densities weighted by the AMS chemical components. A collection efficiency of 0.5 was determined. Detailed investigations and discussions around the collection efficiency of the AMS can be found in the literature (Middlebrook et al., 2012; Dunlea et al., 2009; Kleinman et al., 2008; Drewnick et al., 2004; Quinn et al., 2006). PM_1 is the sum of the mass concentrations of AMS components (OA, NO_3, SO_4 and NH_4). For comparisons of PM_1 from this study and $PM_{2.5}$ EFs from other studies, the mass was estimated between 1 and 2.5 µm to assess the extent of which this might be influencing such comparisons. Using estimated particle mass concentrations from a Fast Cloud Droplet Probe (FCDP) (< 2.5 µm) and those from a UHSAS (<1 µm), there is an estimated 10 % of aerosol mass between 1 and 2.5 µm.

BC The SP2 (Droplet Measurement Technologies) measures the mass of rBC contained in individual aerosols through the laser-induced incandescence of heated rBC-containing aerosols (Stephens et al., 2003; Baumgardner et al., 2004; Schwarz et al., 2006). The SP2 was calibrated using fullerene soot (Alpha Aesar lot# F12S011) (Moteki and Kondo, 2010; Kondo et al., 2011; Laborde et al., 2012) nebulized from a water suspension and passed through an aerosol particle mass analyzer (Kanomax APM3600) to select particles with masses ranging from 0.2 fg/particle to 48 fg/particle. Extremely large

particles containing more than 520 fg of rBC were excluded from analysis due to saturation of the detector (these accounted for only $2x10^{-3}$ % of the total number of rBC containing particles measured by the SP2).

UHSAS Particle size distributions were measured using an Ultra-High Sensitivity Aerosol Spectrometer (UHSAS; Droplet Measurement Technologies). The UHSAS measures the size of individual aerosols passing through a laser beam via Mie scattering (Cai et al., 2008; Kupc et al., 2018). These particles are classified into 99 log-normally spaced bins across the measurement range. Periods where the particle concentration measured by the UHSAS exceeded 3000 particles s^{-1} were excluded from this analysis due to the potential of coincident particles passing through the laser beam. The UHSAS particle sizing was verified using NIST traceable polystyrene latex (PSL) nanospheres of multiple sizes across the measurement range. Total particle mass was calculated from the UHSAS measurements assuming a density of 1.2 g cm^{-3}, based on the proportional density determined from the AMS.

2.1.3 Identification of organic compounds

Three methods were used to provide detailed measurements of gas-phase organic compounds that included the PTRMS, CIMS, and canister samples (AWAS). The PTRMS and CIMS are able to resolve the molecular formula of isobaric species, but cannot distinguish isomers, while the AWAS system can identify and speciate individual compounds. For the PTRMS measurements, compound molecular formulae were assigned based on a limited set of possibilities (particularly for the smaller compounds), known or expected compound sensitivities, and comparing with previously published laboratory work by Koss et al. (2018) based on typical NMOG structures observed in biomass burning emissions. Koss et al. (2018) used a combination of gas-chromatography (GC) pre-separation, NO^+ CIMS and time series correlations to identify 156 compounds measured in biomass burning laboratory experiments with a PTRMS. Additional comparisons were made with PTRMS ion masses reported in Permar et al. (2021) where they used a PTRMS with two GC methods to speciate isomers for some PTRMS ion masses. For formulas with multiple isomer contributions that were not speciated by the PTRMS, or provided by the

AWAS, the fractional contributions in Koss et al. (2018) and Permar et al. (2021) were used to identify the dominant ion and/or contributing compounds. Although the Koss et al. (2018) work was based on laboratory measurements, Permar et al. (2021) found that isomer contributions did not vary much between 24 fires types across the WE-CAN airborne field campaign in western US, which were mainly dominated by fires of pine, fir and spruce trees. For example, in Koss et al. (2018), for the mass spectral ion of C_3H_6O (m/z 58.08), the contribution from acetone was set at 100 % and propanal 0 %, only slightly different from the contribution of 83±6 % for acetone determined by Permar et al., 2021; thus this compound was identified as acetone in this work. Another example is C_4H_8O at m/z 70.091 that has potential contributions from methyl vinyl ketone (MVK), methacrolein and crotonaldehyde, both Koss et al. (2018) and Permar et al. (2021) both reported that MVK is the largest contributor at 48 % and 60±9 % respectively; the compound was labelled here as all three. For C_8H_{10} (m/z 106.168), there are contributions from ethyl benzene, m- and p-xylenes and o-xylene identified as 10%, 68% and 23%, respectively (Koss et al., 2018), with slightly different isomer contributions as per Permar et al. (2021). In this study, as it was not possible to speciate C_8H_{10} with the AWAS system, it is simply identified as C8 aromatics. Similarly, $C_{10}H_{16}$, (m/z 136.238) is identified as total monoterpenes in the present study, with expected contributions from multiple species including alpha and beta pinene, camphene, myrcene, and tricyclene (Permar et al., 2021; Hatch et al., 2017). C_5H_8 at m/z 68.119 was identified as isoprene in the present study, recognizing that there may be a fractional contribution to this mass from methyl-3-buten-2-ol (MBO), although Permar et al. (2021), suggests that MBO may not be significant, based on their analysis of western US wildfires.

For the CIMS, the iodide reagent ion chemistry is most sensitive to polar compounds, particularly carboxylic acids and less sensitive to non-polar compounds (Table S1). Compounds were identified using these known/expected sensitivities and available calibration standards. The AWAS provided speciated measurements of hydrocarbons (<C9), and no oxygenates.

2.1.4 Overlapping compounds There were a number of compounds (or molecular formulae) that were measured by both the PTRMS and the AWAS, as well as compounds that overlapped between the PTRMS and CIMS. Tables S4 and S5 summarize the decisions of overlapping compounds that were retained for derivation of EFs and NERs, as well as for the carbon/nitrogen budget analyses. For the PTRMS and AWAS, for some molecular formulae, the AWAS provided measurements of individual isomers, while the corresponding PTRMS measurement was expected to reflect the sum of those isomers. In deriving EFs and NERs, both the PTRMS and AWAS measurements were included to retain as much information as possible. To avoid double-counting compounds in the carbon and nitrogen budget analyses, only the PTRMS measurement was typically included as it is expected to reflect a sum of all isomers, thus, accounting for more carbon. For example, at the molecular formulas of C_5H_{10}, the PTRMS measurements are expected to reflect the sum of all the isomers, whereas 5 compounds were speciated from the AWAS i.e. c-2-pentene, cyclopentane, 1-pentene, 2-me-1-butene, and 2-me-2-butene. In this case, EFs and NERs were derived for both the PTRMS and AWAS measurements, but only the PTRMS measurements were included in the budget analyses.

Between the PTRMS and CIMS, there were 18 overlapping molecular formulae of which 4 were identified as the same compound. The CIMS measurements were retained for 3 of these 4 compounds (Table S5) because they were directly calibrated (Table S2), whereas the PTRMS compounds were calculated. For the 4th compound (acetic acid), EFs for both instruments were reported, but only the CIMS data for acetic acid were included in the carbon budget analyses; EFs were very similar (Table A1). The remaining overlapping formulae between the CIMS and PTRMS were calibrated with different analytes, and thus assumed to be different species. While there may in fact be some overlap between isomers contributing to these formulae, their overall contribution to the TC budget is small (<4 %). An attempt was made to quantify as many other peaks that were present in the CIMS mass spectra as possible and apply sensitivity factors. However, the available sensitivity factors were based on laboratory experiments investigating anthropogenic emissions and highly uncertain for biomass burning measurements. Nevertheless, application of these sensitivity factors resulted in average mass from the

CIMS spectra totalling < 1.5 % of the TC, so although uncertain, exclusion of these masses is not expected to significantly influence the total carbon budget. It is assumed that all the acids measured by the CIMS are non-aromatic for classifying into chemical structural categories.

2.2 Flight and fire description

The 18BN-Larry fire (the Lac LaLoche fires) was detected by the Saskatchewan wildfire management agency on June 23, 2018. Satellite images showed fire hot spots on June 23 and by the evening of June 23 it grew to 1,250 hectares (ha) and to 2,600 ha on June 24th. On the morning of June 25, 2018, there was a very weak nocturnal inversion and moderately strong south to southeast winds at 33 knots above the inversion. The range of fire intensities during the previous night, as well as the observed high humidity (80-90 %) and light to moderate winds observed at the surface also indicates that the fire source at the time of aircraft sampling was in a smoldering combustion state. Flight tracks were flown at Lagrangian distances downwind of the wildfire. Multiple passes (i.e. transects) perpendicular to the plume direction were made at different altitudes. Two plumes were identified: the SP was clearly due to the fire hot spots identified by MODIS (green dots encompassed by a polygon), but the source of the NP is less certain. It is possible that MODIS was unable to detect the fire source because the fire heat signature was below the threshold for satellite instrument detection. However, surface wind measurements at Lac LaLoche (SI Table S1 in McLagan et al., 2021) show that the wind direction was southerly just prior (approx. 30 min) to the start of the aircraft measurements, and then shifted to southeast (135+/-13°) for the duration of the aircraft flight. Therefore, it is likely that the NP was from the same fire source as the SP that had been transported in a northerly direction just prior to aircraft sampling, and subsequently moved to a northwesterly direction with the wind change. The width of the SP and NP was approximately 14-37 km separated by approximately 8-19 km depending on the sampling altitude, and with an aircraft speed of ~90 m s^{-1}, the plumes were traversed in 3-7 min (Fig. 2).

3 Emission ratios, emission factors and combustion efficiency

3.1 Combustion state

The combustion efficiency (CE) can be used to characterize and compare the combustion state of the fire, (i.e. the fraction of fuel carbon converted to atmospheric CO_2) (Ward and Radke, 1993). The CE is dependent upon many factors including fire combustion state, fuel chemistry, fuel geometry, growth stage, moisture content and meteorological conditions such as wind speed and temperature. In a flaming fire, high temperature reactions tend to go to completion (>90 %) as rapid reaction of O_2 with the fuel C, H, N and S produces highly oxidized gases including CO_2, NO_x, and SO_2 and BC. As a fire progresses, incomplete combustion characteristics of smoldering fires becomes more dominant resulting in a larger proportion of the emitted carbon in the form of CO, CH_4, NMOC, and OA. Airborne measurements tend to sample a mixture of combustion states; however, there tends to be a dominant phase of combustion at different fire stages (Andreae and Merlet, 2001). If only accounting for CO_2 and CO, the MCE for the SP is 0.90±0.01 and NP is 0.88±0.01, higher than the CE by 7.1 % and 6.6 % for the SP and NP, respectively. These differences are driven mostly by the additional contribution from NMOGs indicating the importance of their inclusion in assessing fire combustion state.

Since the flaming phase was likely more than 14 hrs prior to aircraft sampling, it is possible that the emissions from this fire may also reflect a residual smoldering combustion (RSC) component. RSC produces emissions from combustion of forest floor and woody debris that are not associated with flaming, can be sustained for long periods of time after the passage of a flame front, and are not strongly lofted through fire-induced convection (Bertschi et al., 2003). It is noted though that observations of increased levels of flaming compounds in the plumes including CO_2 and BC (Fig. S2) suggest that to some extent, flaming processes also contributed to the release of these compounds. It is likely that different parts of the fire had varying mixtures of smoldering, flaming and residual combustion processes, but the evidence strongly suggests that the Lac LaLoche fire was predominantly in a smoldering combustion state during the aircraft measurement time period. Smoldering fires can create persistent and poorly ventilated smoke that can be a significant driver in remote community evacuations (McGee, 2020).

In addition, boreal fires in this region tend to exhibit a large component of smoldering combustion which can consume large amounts of above and below ground biomass (Akagi et al., 2011).

311 Table S1. Measurements with associated instrument, principle of operation, sampling time resolution and
312 applicable method references.

Measurement	**Instrument**	**Principle of measurement**	**Time Resolution (s)**	**Uncertainty**	**Reference**
NO	Thermo 42i	Chemiluminescence with O_3	1	±5 %	Clyne at al., 1964 Ridley et al., 1990
NO_2	Thermo 42i	Photolysis + chemiluminescence with O_3	1	±7 %	Penkett et al., 2011
NO_y	Thermo 42i	Heated (350°C) and molybdenum catalyzed conversion + chemiluminescence with O_3	1	±5 %	Fehsenfeld et al., 1987; Williams et al., 1998
SO_2	Thermo 43i	UV pulsed fluorescence	1	±5 %	Stecher et al., 1997
O_3	Thermo 42i	Chemiluminescence	1	±5 %	N/A
NH_3	LGR model 911-0039	Absorption	1	±5 %	Leifer et al., 2017
Hg	Tekran 237X	Fluorescence	120		Cole et al., 2014; McLagan et al., 2021
CO, CO_2, CH_4	Picarro G-2401-m	Cavity ring down spectrometry	2	CH_4 ~3 ppb at background	Baray et al., 2018
Total Carbon (TC)	Picarro G-2401-m	Heated (650°C) platinum catalyzed conversion to CO_2	2		Stockwell et al., 2018; Veres et al., 2010.
Total non-methane organic gases ($NMOG_T$)	Picarro G-2401-m x 2	Difference method, heated (650°C) platinum catalyzed conversion to CO_2	10		Stockwell et al., 2018; Veres et al., 2010
VOCs	CIMS	Chemical ionization/mass spectrometry	1	10-50% compound dependent	Liggio et al., 2017; Lee et al., 2014
VOCs	Canister grab samples	Grab samples/GC with MS and FID analysis	Grab	40 %	
VOCs	PTRMS	Proton transfer/ionization/mass spectrometry	1	VOCs with available standards: 15-20%; Calculated VOCs: 50%	Li et al., 2017; Sekimoto et al., 2017
VOCs-SVOCs (C10-C25)	Custom packed adsorbent tubes	Offline analysis with TD-GC-APCI-Q-ToF	Variable (245-3140 sec per tube)		Sheu et al., 2018; Khare et al., 2019; Ditto et al., 2021

Particle chemical composition	Aerosol mass spectrometer	Volatilization, ionization and mass spectrometry	10	OA: 35% SO_4:25% NO_3:20% NH_4:25%	DeCarlo et al., 2008; Jimenez et al., 2003; Allan et al., 2003
Black carbon	SP2	Incandescence	1		Stephens et al., 2003; Baumgardner et al., 2004; Schwarz et al., 2006
Particle size distributions (60 -1000 nm)	Ultra-High Sensitivity Aerosol Spectrometer (UHSAS)	Particle light scattering	1		Cai et al., 2008; Kupc et al., 2018

Table S2. Standards used to calibrate the CIMS. The iodide chemistry is most sensitive to polar compounds and less sensitive to non-polar compounds. The sensitivity tends to increase for keto-, hydroxy- and acid groups, in order. Most of the keto- groups are attached to a carboxylic acid. For the larger acids (>C4) where there can be several isomers, they are generally identified as saturated C4 carboxylic acids and unsaturated C5 acids.

Molecular weight	Molecular formula	Compound Name	Calibration standard	Calibration Source	Reference
27.026	HCN	hydrogen cyanide	Hydrogen Cyanide	High Pressure Cylinder (Air Liquide)	Stockwell et al 2018
32.06	SO_2	sulphur dioxide	Sulfur Dioxide	High Pressure Cylinder (Air Liquide)	Lee et al 2018
43.025	HNCO	isocyanic acid	Isocyanic Acid	Thermal Decomposition/Diffusion	Roberts et al 2010
46.025	CH_2O_2	formic acid	Formic Acid	Liquid Standard supplied by Liquid Calibration Unit (LCU)	Mungall et al 2017
47.013	HNO_2	nitrous acid	Nitrous Acid	Acid Displacement (output quantified by ion chromatography)	Roberts et al 2010
57.052	C_2H_3NO	hydroxy acetonitrile	Glycolic Acid Nitrile	Liquid Standard supplied by Liquid Calibration Unit (LCU)	Mungall et al 2017
60.052	$C_2H_4O_2$	acetic acid	Acetic Acid	Liquid Standard supplied by Liquid Calibration Unit (LCU)	Mungall et al 2017
63.012	HNO_3	nitric acid	Nitric Acid	Permeation Tube (output quantified by ion chromatography)	Neuman et al 1999
72.063	$C_3H_4O_2$	acrylic acid	Acrylic Acid	Liquid Standard supplied by Liquid Calibration Unit (LCU)	Mungall et al 2017
74.079	$C_3H_6O_2$	propionic acid	Propionic Acid	Liquid Standard supplied by Liquid Calibration Unit (LCU)	Mungall et al 2017
79.011	HNO_4	pernitric acid	Pernitric Acid	Reaction of HO_2 with NO_2 (quantified by thermal decomposition Cavity Ringdown Spectroscopy of NO_2)	Veres et al 2015
84.074	$C_4H_4O_2$	c4h4o2	2(5H)-Furanone	Liquid Standard supplied by Liquid Calibration Unit (LCU)	Mungall et al 2017
85.062	$C_3H_3NO_2$	cyanoacetic acid	Cyanoacetic Acid	Liquid Standard supplied by Liquid Calibration Unit (LCU)	Mungall et al 2017
86.09	$C_4H_6O_2$	methacrylic acid	Methacrylic Acid	Liquid Standard supplied by Liquid Calibration Unit (LCU)	Mungall et al 2017

88.062	$C_3H_4O_3$	pyruvic acid	Pyruvic Acid	Liquid Standard supplied by Liquid Calibration Unit (LCU)	Mungall et al 2017
88.106	$C_4H_8O_2$	C4 saturated carboxylic acids	Butyric Acid	Liquid Standard supplied by Liquid Calibration Unit (LCU)	Mungall et al 2017
91.066	$C_2H_5NO_3$	C2 Nitro alcohol	2-Nitroethanol	Liquid Standard supplied by Liquid Calibration Unit (LCU)	Mungall et al 2017
100.117	$C_5H_8O_2$	unsaturated C5 carboxylic acids	4-Pentenoic Acid	Liquid Standard supplied by Liquid Calibration Unit (LCU)	Mungall et al 2017
102.089	$C_4H_6O_3$	C4 oxo-carboxylic acids	2-Ketobutyric Acid	Liquid Standard supplied by Liquid Calibration Unit (LCU)	Mungall et al 2017
102.133	$C_5H_{10}O_2$	C5 saturated carboxylic acids	Valeric Acid + Isovaleric Acid (equal parts)	Liquid Standard supplied by Liquid Calibration Unit (LCU)	Mungall et al 2017
104.105	$C_4H_8O_3$	C4 hydroxy-carboxylic acids	3-Hydroxybutyric Acid	Liquid Standard supplied by Liquid Calibration Unit (LCU)	Mungall et al 2017
108.009	N_2O_5	dinitrogen pentoxide	Dinitrogen Pentaoxide	Titration of NO_2 with O_3 (quantified by thermal decomposition Cavity Ringdown Spectroscopy of NO_2)	Lee et al 2018
114.144	$C_6H_{10}O_2$	sum of cyclic saturated and n-unsaturated C5 carboxylic acids	Cyclopentanecarboxylic Acid	Liquid Standard supplied by Liquid Calibration Unit (LCU)	Mungall et al 2017
116.116	$C_5H_8O_3$	C5 oxo-carboxylic acids	Levulinic Acid	Liquid Standard supplied by Liquid Calibration Unit (LCU)	Mungall et al 2017
116.16	$C_6H_{12}O_2$	C6 saturated carboxylic acids	Hexanoic Acid + 4-Methyl-Valeric Acid (equal parts)	Liquid Standard supplied by Liquid Calibration Unit (LCU)	Mungall et al 2017
118.132	$C_5H_{10}O_3$	C5 hydroxy-carboxylic acids	2-Hydroxy-2-methylbutyric Acid	Liquid Standard supplied by Liquid Calibration Unit (LCU)	

126.155	$C_7H_{10}O_2$	unsaturated C6 cyclic carboxylic acid	3-Cyclohexene-1-carboxylic Acid	Liquid Standard supplied by Liquid Calibration Unit (LCU)	
128.171	$C_7H_{12}O_2$	C6 unsaturated carboxylic acids	6-Heptenoic Acid	Liquid Standard supplied by Liquid Calibration Unit (LCU)	
130.187	$C_7H_{14}O_2$	C7 saturated carboxylic acids	Heptanoic Acid	Liquid Standard supplied by Liquid Calibration Unit (LCU)	
132.159	$C_6H_{12}O_3$	C6 hydroxy-carboxylic acids	2-Hydroxyisocaproic Acid	Liquid Standard supplied by Liquid Calibration Unit (LCU)	

339

340

Table S3. Standards used to calibrate the PTRMS. [a]C8 aromatics - expected contributions from ethyl benzene, m- and p-xylenes and o-xylene. [b]Monoterpenes - expected contributions from camphene, α-pinene, β-pinene, myrcene, and tricyclene.

Molecular weight	Molecular formula	Compound Name	Calibration standard
30.026	CH_2O	formaldehyde	formaldehyde
32.042	CH_4O	methanol	methanol
34.076	H_2S	hydrogen sulfide	hydrogen sulfide
41.053	C_2H_3N	acetonitrile	acetonitrile
44.053	C_2H_4O	acetaldehyde	acetaldehyde
56.064	C_3H_4O	acrolein	acrolein
58.08	C_3H_6O	acetone	acetone
62.13	C_2H_6S	dimethyl sulfide	dimethyl sulfide
68.119	C_5H_8	isoprene	isoprene
70.091	C_4H_6O	MVK, methacrolein, crotonaldehyde	crotonaldehyde
72.107	C_4H_8O	MEK, 2-methyl acetate, ethyl formate	methylethyl ketone
76.157	C_3H_8S	2-propanethiol, ethyl methyl sulfide	ethylmethyl sulfide
78.114	C_6H_6	benzene	benzene
84.136	C_4H_4S	thiophene	thiophene
90.184	$C_4H_{10}S$	diethyl sulfide, butanethiol	diethyl sulfide
92.141	C_7H_8	toluene	toluene
98.163	C_5H_6S	methyl thiophene	2-methylthiophene
106.168	C_8H_{10}	C8 aromatics[a]	o-xylene
112.19	C_6H_8S	dimethylthiophene	2,3-dimethylthiophene
136.238	$C_{10}H_{16}$	monoterpenes[b]	camphene

346 Table S4. Overlapping compounds measured between the PTRMS and AWAS.

Molecular Weight	Formula	Compound Name	Instrument	Decision for budget	Decision for EFs
42.081	C_3H_6	propene	AWAS and PTRMS	AWAS	AWAS
54.092	C_4H_6	butadiene/fragments	PTRMS	PTRMS	PTRMS and AWAS
		1,3-butadiene	AWAS		
56.108	C_4H_8	butenes	PTRMS	AWAS	AWAS
		cis-2-butene	AWAS		
		isobutene	AWAS		
		trans-2-butene	AWAS		
		1-butene	AWAS		
58.124	C_4H_{10}	butanes	PTRMS	AWAS	AWAS
		isobutane	AWAS		
		n-butane	AWAS		
70.135	C_5H_{10}	pentene/fragments	PTRMS	PTR	PTRMS and AWAS
		cis-2-pentene	AWAS		
		cyclopentane	AWAS		
		1-pentene	AWAS		
		2-methyl-1-butene	AWAS		
		2-methyl-2-butene	AWAS		
78.114	C_6H_6	benzene	PTRMS and AWAS	PTRMS	PTRMS
82.146	C_6H_{10}	cyclohexene	PTRMS and AWAS	PTRMS	PTRMS
84.162	C_6H_{12}	hexene	PTRMS and AWAS	PTRMS (hexane) AWAS (cyclohexane)	PTRMS (hexane) AWAS (cyclohexane)
		cyclohexane	AWAS		
86.178	C_6H_{14}	hexanes	PTRMS and AWAS	AWAS	AWAS
		n-hexane	AWAS		
		2,3-dimethyl butane	AWAS		
		2,3-dimethylpentane	AWAS		

347

348

349

350

351

Table S5. Overlapping compounds measured between the PTRMS and CIMS. [a]The PTRMS signal at molecular weight 60.052 is reported as acetic acid fragment; the signal can also be due to glycoaldehyde (Koss et al., 2018), but the PTRMS and CIMS acetic acid mixing ratios and EFs match each other closely suggesting that the PTRMS fragment is mostly due to acetic acid.

Molecular weight	Formula	CIMS compound name	PTRMS compound name	Decision
43.025	HNCO	Isocyanic acid	Isocyanic acid	CIMS and PTRMS for reporting EF and ER; CIMS for carbon budget
46.025	CH_2O_2	Formic acid	Formic acid	CIMS
57.052	C_2H_3NO	Hydroxy acetonitrile	Methyl isocyanate	CIMS and PTRMS
60.052	$C_2H_4O_2$	Acetic acid	Acetic acid fragment[a]	CIMS and PTRMS for reporting EF and ER; CIMS for carbon budget
72.063	$C_3H_4O_2$	Acrylic acid	Methyl glyoxal/acrylic acid	CIMS
74.079	$C_3H_6O_2$	Propionic acid	Hydroxy acetone/ethyl formate	CIMS and PTRMS
84.074	$C_4H_4O_2$	Unidentified	Furanone	CIMS and PTRMS
85.062	$C_3H_3NO_2$	Cyanoacetic acid	Methyl cyanoformate	CIMS and PTRMS
86.09	$C_4H_6O_2$	Methacrylic acid	Butanedione/isomers	CIMS and PTRMS
88.062	$C_3H_4O_3$	Pyruvic acid	Pyruvic acid	CIMS
88.106	$C_4H_8O_2$	C4 saturated carboxylic acids	Methyl propanoate	CIMS and PTRMS
100.117	$C_5H_8O_2$	Unsaturated C5 carboxylic acids	Methyl methacrylate/isomers	CIMS and PTRMS
102.089	$C_4H_6O_3$	C4 oxo-carboxylic acids	Acetic anhydride	CIMS and PTRMS
102.133	$C_5H_{10}O_2$	C5 saturated carboxylic acids	Valeric acid	CIMS and PTRMS
114.144	$C_6H_{10}O_2$	Sum of cyclic saturated and n-saturated C5 carboxylic acids	Caprolactone/c6 esters/c6diketone isomers	CIMS and PTRMS
116.16	$C_6H_{12}O_2$	C6 carboxylic acids	Butyl acetate/c6 esters	CIMS and PTRMS
118.132	$C_7H_{10}O_2$	Unsaturated C6 cyclic carboxylic acids	Cyclohexene carboxylic acid	CIMS and PTRMS
128.171	$C_7H_{12}O_2$	C6 unsaturated carboxylic acids	Cyclohexanoic acid	CIMS and PTRMS
130.187	$C_7H_{14}O_2$	C7 saturated carboxylic acids	Amyl acetate	CIMS and PTRMS

Table S6. Compounds with no significant observed emissions

Molecular Weight	Formula	Compound Name	Instrument
34.08	H_2S	hydrogen sulfide	PTRMS
70.05	$C_2H_3O_2$	Propiolic acid	PTRMS
72.17	C_5H_{12}	2,2-dimethylpropane	AWAS
82.06	$C_4H_2O_2$	cyclobutenedione	PTRMS
85.06	$C_3H_3NO_2$	cyanoacetic acid	CIMS
86.2	C_6H_{14}	2,2-dimethylbutane	AWAS
91.07	$C_2H_5NO_3$	C2 nitro alcohol	CIMS
100.07	$C_4H_4O_3$	dihydro furandione	PTRMS
102.195	$C_5H_{10}S$	cyclopentanethiol	PTRMS
104.105	$C_4H_8O_3$	C4 hydroxy-carboxylic acids	CIMS
112.24	C8H16	cis-1,2-dimethylcyclohexane	AWAS
112.56	C_6H_5Cl	chlorobenzene	PTRMS
118.13	$C_5H_{10}O_3$	C5 hydroxy-carboxylic acids	CIMS
128.29	C9H20	2,5-dimethylheptane	AWAS
134.24	C10H14	1-methyl-2-n-propylbenzene	AWAS
140.25	$C_8H_{12}S$	butylthiophene	PTRMS
142.32	C10H22	2,2-dimethyloctane	AWAS
147.00	$C_6H_4Cl_2$	dichlorobenzene	PTRMS
154.12	$C_7H_6O_4$	dihydroxybenzoic acid	PTRMS
n/a	Cl^-	p-chloride	AMS

Table S7. Emission ratios (relative to CO, as μg m^{-3} per μg m^{-3} CO) for complex mixtures of gas-phase CH, CHO_1, and CHS_1 compounds grouped by carbon number for all targeted molecular formulas, derived from the integrated cartridge samples, using the sample taken across the lowest transects of Screen 1. Note: based on flight design, it was not possible to directly derive emission factors due to the lack of background cartridge samples in the upwind region of the fire so ratios to CO in the concentrated lower (Screen 1) transects are used in the analysis to approximate emission factors from the wildfire.

Carbon Number	CH in-plume ratio to CO	CHO_1 in-plume ratio to CO	CHS_1 in-plume ratio to CO
10	7.65E-03	2.28E-03	5.59E-06
11	0.00E+00	4.71E-04	1.15E-05
12	3.86E-05	5.23E-04	1.73E-06
13	1.71E-04	3.84E-04	9.74E-06
14	1.11E-04	7.65E-04	4.15E-06
15	2.62E-04	7.12E-04	1.67E-05
16	8.05E-04	4.96E-04	4.85E-05
17	8.70E-04	1.33E-03	2.42E-04
18	1.20E-03	9.05E-04	8.43E-05
19	1.37E-03	8.46E-04	3.04E-04
20	2.01E-03	6.48E-04	1.01E-04
21	1.77E-03	3.66E-04	2.05E-04
22	2.85E-03	2.31E-04	6.34E-05
23	1.58E-03	1.06E-04	2.08E-05
24	7.24E-04	8.68E-05	4.28E-05
25	3.03E-04	3.92E-05	4.36E-05

Table S8. Compounds shown in Figure 7 where the identifications/naming are not exact matches with the current study. 1 Individually identified compounds were summed for comparison to the present study; 2 Each compound was compared with the value from the present study.

Molecular Weight	Compound	Instrument	Compound Name	Andreae Names	Koss Names	Permar Names	Urbanski Names
54.092	C_4H_6	PTRMS	butadiene/fragments	butadiene	1,3-butadiene + 1,2-butadiene	1,3-butadiene, 1,2-butadiene	n/a
54.092	C_4H_6	AWAS	1,3-butadiene	butadiene	1,3-butadiene + 1,2-butadiene	1,3-butadiene, 1,2-butadiene	n/a
57.052	C_2H_3NO	CIMS	hydroxy acetonitrile	n/a	methyl isocyanate + hydroxyacetonitrile	methyl isocyanate, hydroxyacetonitrile	n/a
58.124	C_4H_{10}	AWAS	isobutane	n/a	n/a	n-Butane	n/a
60.052	$C_2H_4O_2$	CIMS	acetic acid	Acetic acid	acetic acid + glycolaldehyde	acetic acid, glycolaldehyde (=hydroxylacetaldehyde)	n/a
60.096	C_3H_8O	PTRMS	propanol	n/a	n/a	Isopropanol	n/a
66.103	C_5H_6	PTRMS	cyclopentandiene	n/a	n/a	1,3-cyclopentadiene	1,3-CyclopentadienePIT
70.091	C_4H_6O	PTRMS	MVK, methacrolein, crotonaldehyde	Methacrolein	MVK + methacrolein + crotonaldehyde	Methyl vinyl ketone, Methacrolein, 2-Butenal (=crotonaldehyde)	[1]Crotonaldehyde + Methacrolein + Methyl Vinyl Ketone MVK
70.135	C_5H_{10}	PTRMS	pentene/methyl butene/fragments	1-Pentene + 2-pentene	pentene+methyl butene	pentenes, methylbutenes	n/a
70.135	C_5H_{10}	AWAS	c-2-pentene	2 pentene cis&tran	pentene+methyl butene	pentenes, methylbutenes	n/a
70.135	C_5H_{10}	AWAS	cyclopentane			cyclopentane	n/a
70.135	C_5H_{10}	AWAS	pentene	1-Pentene	pentene+methyl butene	pentenes, methylbutenes	n/a
70.135	C_5H_{10}	AWAS	methyl-1-butene	1-Pentene	pentene+methyl butene	pentenes, methylbutenes	n/a
70.135	C_5H_{10}	AWAS	methyl-2-butene	1-Pentene	pentene+methyl butene	pentenes, methylbutenes	n/a
72.063	$C_3H_4O_2$	CIMS	acrylic acid	n/a	n/a	pyruvaldehyde (=methyl glyoxal), acrylic acid	n/a
72.107	C_4H_8O	PTRMS	methy ethyl ketone + butanal + 2-methylpropanal	2-butanone (methyl ethyl ketone)	methyl ethyl ketone + butanal + 2-methylpropanal	methyl ethyl ketone, 2-methylpropanal, butanal	[1]Methyl Ethyl Ketone MEK + n-Butanal + 2-

							Methylpropanal
72.151	C_5H_{12}	AWAS	methylbutane	n/a	n/a	n-pentane	n/a
74.079	$C_3H_6O_2$	PTRMS	hydroxy acetone/ethyl formate	n/a	methyl acetate + ethyl formate + hydroxyacetone	Hydroxyacetone, Methyl acetate, Ethyl formate	Ethyl Formate
81.118	C_5H_7N	PTRMS	pentene nitriles/methyl pyrrole	n/a	n/a	n/a	1-Methylpyrrole
82.102	C_5H_6O	PTRMS	methyl furan	n/a	2-methylfuran + 3-methylfuran + general HCO	2-Methylfuran, 3-Methylfuran	[2]2-Methylfuran, 3-Methylfuran
84.118	C_5H_8O	PTRMS	cyclopentanone/ isomers	n/a	3-methyl-3-butene-2-one + cyclopentanone + HCO1 isomers	3-Methyl-3-buten-2-one, Cyclopentanone	Cyclopentanone
84.162	C_6H_{12}	PTRMS	hexene/fragments	1-hexene	n/a	n/a	[2]1-Hexene, cis-2-Hexene
86.09	$C_4H_6O_2$	PTRMS	butanedione/ isomers	2,3-butanedione	2,3-butanedione + methyl acrylate + other HCO2	2,3-butanedione, methyl acrylate	2,3-Butadione
86.134	$C_5H_{10}O$	PTRMS	pentanone	n/a	n/a	n/a	[2]2-Pentanone, 3-Pentanone
86.178	C_6H_{14}	AWAS	2,3-methylpentane	n/a	n/a	3-methylpentane	3-Methylpentane
96.085	$C_5H_4O_2$	PTRMS	furfural	furfural (2-furaldehyde)	2-furfural + 3-furfural + other HCO2	2-furfural (=furaldehyde), 3-furfural	2-Furaldehyde
98.189	C_7H_{14}	PTRMS	heptene	n/a	n/a	n/a	1-Heptene
100.117	$C_5H_8O_2$	PTRMS	methyl methacrylate / isomers	n/a	Methyl methacrylate + other HCO2	Methyl methacrylate	Methyl Methacrylate
100.161	$C_6H_{12}O$	PTRMS	hexanal/hexanones	n/a	hexanal + hexanones	Hexanones, Hexanal	[1]n-Hexanal + Hexanones
103.124	C_7H_5N	PTRMS	benzonitrile	n/a	Benzonitrile	Benzonitrile	Benzenenitrile
106.168	C_8H_{10}	PTRMS	C8 aromatics	n/a	Ethyl benzene + m-xylene + p-	C8 Aromatics	[1]Ethylbenzene + m,p-Xylenes + o-Xylene

					xylene + o-xylene		
112.216	C_8H_{16}	PTRMS	octene	n/a	n/a	n/a	1-Octene
118.135	C_8H_6O	PTRMS	benzofuran	n/a	Benzofuran	Benzofuran	BenzofuranPIT
118.179	C_9H_{10}	PTRMS	methylstyrenes/ propenyl benzenes	n/a	Indane + methyl styrenes + propenyl benzenes	Methylstyrenes, Indane, Propenylbenzenes	[1]1-Propenylbenzene, 2-Methylstyrene, 2-Propenylbenzene, 3-Methylstyrene, 4-Methylstyrene, alpha-Methylstyrene
120.195	C_9H	PTRMS	C9 aromatics	1,2,3-trimethylbenzen, 1,2,4-trimethylbenzen, 1,3,5-trimethylbenzene (Simpson et al., 2011)	C9 aromatics	C9 aromatics	[1]1,2,3-Trimethylbenzene, 1,2,4-Trimethylbenzene, 1,3,5-Trimethylbenzene, 1-Ethyl-2-Methylbenzene, 1-Ethyl-3-,4-Methylbenzene, Isopropylbenzene, n-Propylbenzene
132.162	C_9H_8O	PTRMS	methyl benzo furans	n/a	Methyl benzofuran	Methylbenzofurans	[1]Methylbenzofuran isomer 1, Methylbenzofuran isomer 2, Methylbenzofuran isomer 3
132.206	$C_{10}H_{12}$	PTRMS	ethyl styrene/ methyl propenyl benzene	n/a	Methyl propenyl benzene + ethyl styrene	Ethyl styrenes, Methylpropenylbenzenes, Butenylbenzenes	[1]1-Methyl-1-Propenylbenzene, Ethylstyrene
134.222	$C_{10}H_{14}$	PTRMS	C10 Aromatics	n/a	C10 Aromatics	C10 Aromatics	[1]1,4-Diethylbenzene,

							1-Butenylbenzene, Ethyl Xylene isomer 1, Ethyl Xylene isomer 2, Isobutylbenzene, Methyl-n-Propylbenzene isomer 1, Methyl-n-Propylbenzene isomer 2, n-Butylbenzene, p-Cymene
136.238	$C_{10}H_{16}$	PTRMS	monoterpenes	sum of alpha + beta-pinene (Simpson et al., 2011)	monoterpenes	monoterpenes	n/a
148.249	$C_{11}H_{16}$	PTRMS	C11 aromatics/ pentamethylbenzene	n/a	n/a	n/a	C11 Aromatics

394

395

Table S9. Emission speciation profile for SAPRC11 chemical mechanism derived from normalized EFs from the present study and compared with wildfire smoldering emission speciation profile from the EPA SPECIATEv4.5 #95428 dataset. Note that SESQ (sesquiterpene), WSOC (water soluble organic carbon) and IVOC are non-standard SAPRC11 mechanism species. Please refer to Carter and Heo (2013) for mechanism species definition.

SAPRC11 Lumped Species Name	**Molecular Weight (g/mol)**	**Normalized Mass Fraction (Hayden et al.)**	**Normalized Mass Fraction (SPECIATEv4.5 #95428)**
CCOOH	60.05	0.052	0.031
ACET	58.08	0.012	0.0072
ACYL	26.03728	0.0042	0.00059
ALK1	30.07	0.021	0.011
ALK2	36.73	0.0098	0.0043
ALK3	58.61	0.011	0.0077
ALK4	77.6	0.0035	0.030
ALK5	118.89	0.0032	0.28
ARO1	95.16	0.016	0.034
ARO2	118.72	0.022	0.067
BACL	86.09	0.013	0.0050
BALD	106.13	0.0010	0.0034
BENZ	78.11	0.0071	0.0035
CATL	110.11064	0.0017	0.014
CCHO	44.05	0.017	0.023
CH4	16.043	0.13	0.044
CRES	108.14	0.0014	0.0027
ETHE	28.05	0.023	0.0065
HCOOH	46.03	0.0026	0.0038
GLY			0.000046
HCHO	30.03	0.016	0.0084
IPRD	100.12	0.00010	0.0037
ISOP	68.12	0.0064	0.00041
MACR	70.09	0.0054	0.0044
MEK	72.11	0.0035	0.0028
MEOH	32.04	0.030	0.016
MGLY			0.000037
MVK	70.09	0.0030	0.019
NROG	1	0.00017	0.13
NVOL	1	0.000010	
OLE1	72.34	0.045	0.049
OLE2	75.78	0.0063	0.025
PACD	74.08	0.019	0.00047
PHEN	94.11124	0.0029	0.0054
PROD2	116.16	0.0023	0.027

RCHO	58.08	0.00015	0.0035
TERP	136.24	0.0061	0.032
XYNL	122.1644	0.00043	
SESQ	204.35	0.000033	
WSOC	227	0.056	
IVOC	227.3333333	0.042	

401

402

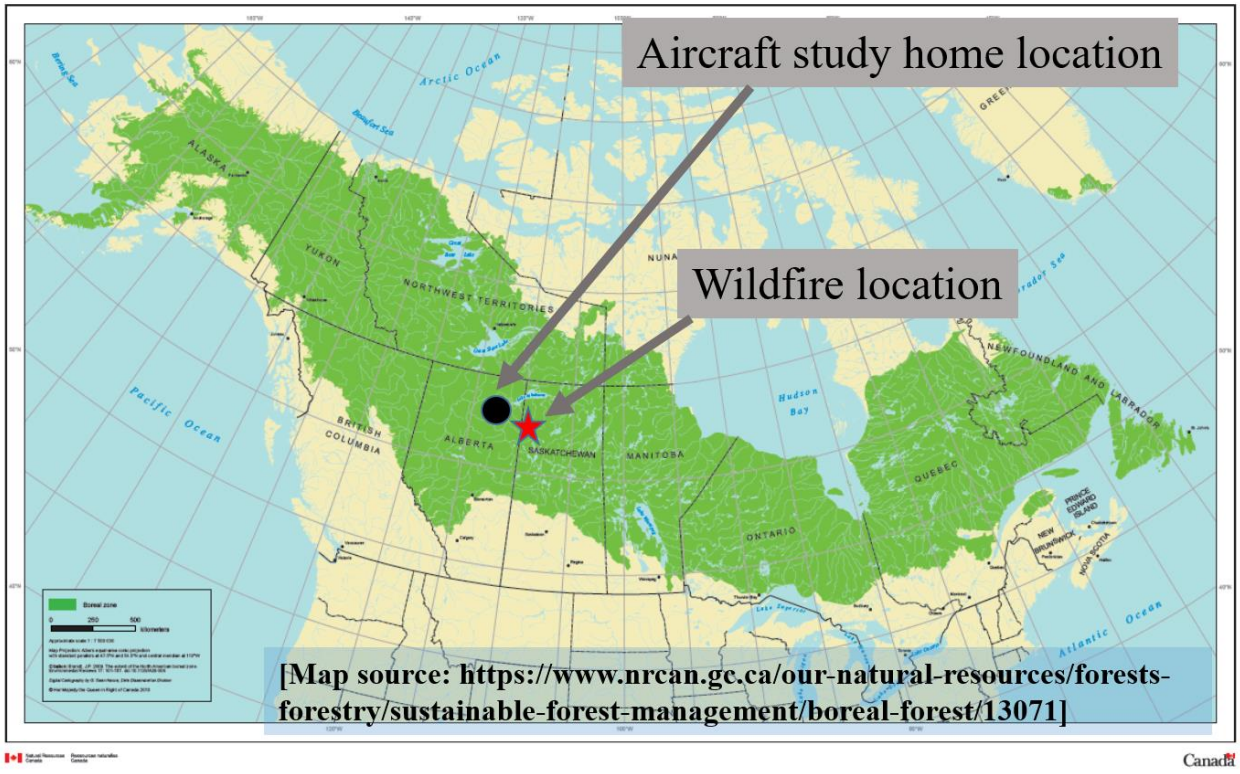

Figure S1. Map showing the home location of the airborne study at Fort McMurray, Alberta and the location of the wildfire in Saskatchewan. The green shaded region shows the extent of the boreal forest coverage across Canada and Alaska.

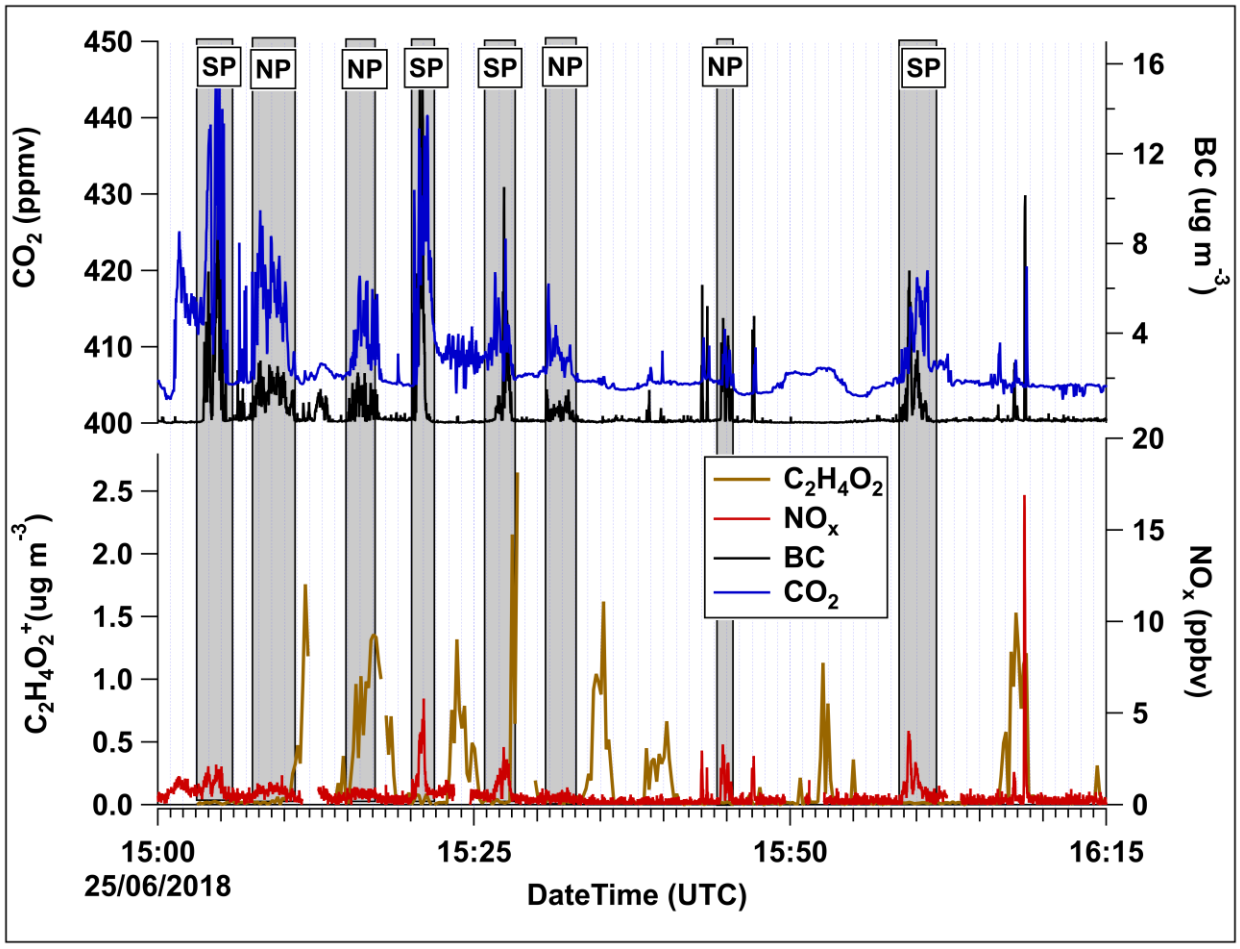

Figure S2. Time series of CO_2, BC and NO_x mixing ratios, and $C_2H_4O_2^+$ (levoglucosan fragment derived from the AMS) concentrations for Screen 1. The in-plume portions are indicated by the vertical grey bars. The aircraft flew back and forth across the plumes at increasing altitudes to complete five transects; a transect represents one pass across the SP and NP at the same altitude.

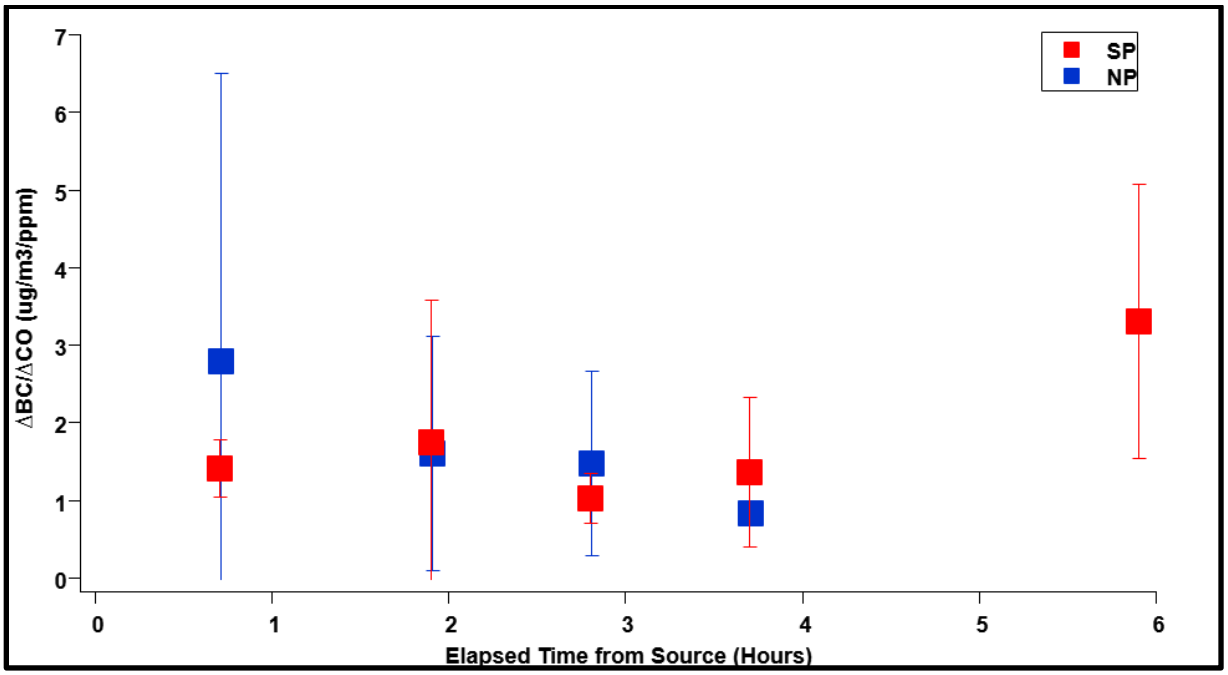

Figure S3. Using ΔBC/ΔCO (Selimovic et al., 2019) as an indicator of plume mixing downwind of the Lac LaLoche fire. The squares show the average and the vertical lines the standard deviation for the transects within the mixed layer for each screen.

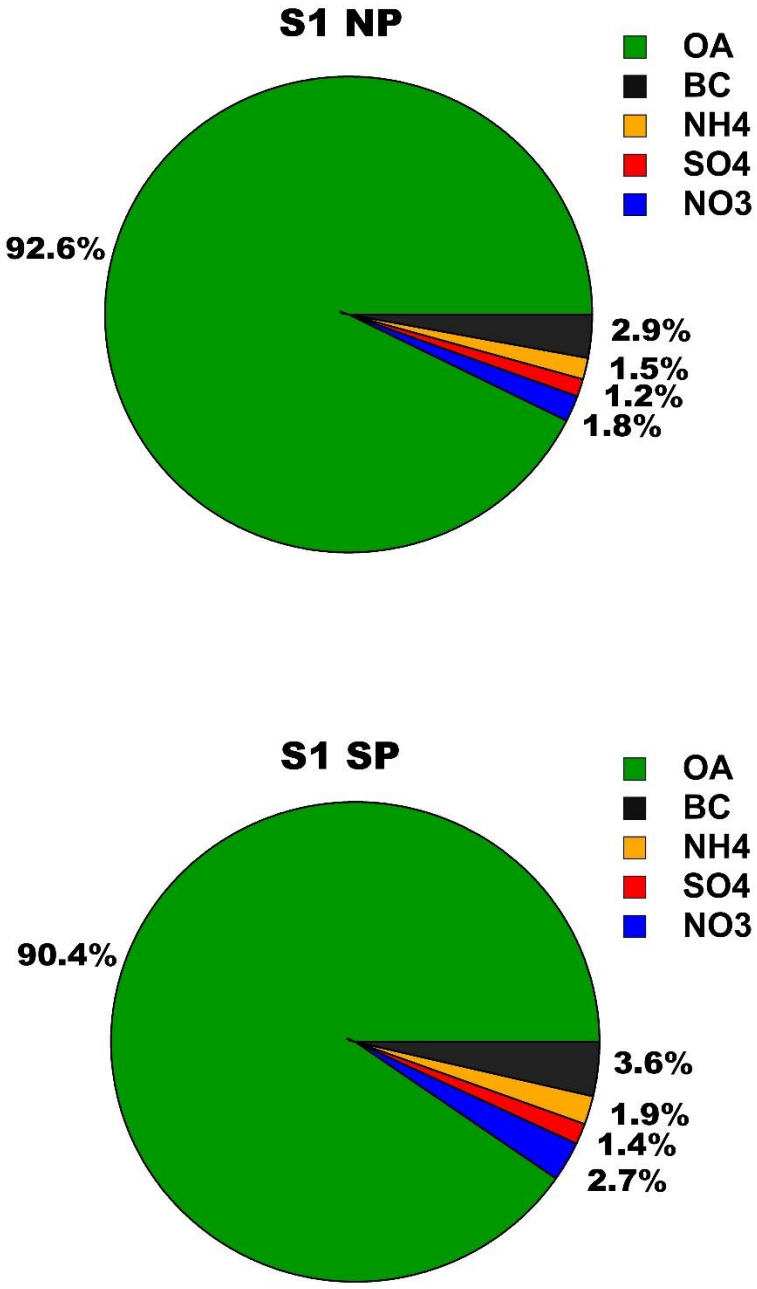

Figure S4. Percent contribution from individually measured particle-phase species for the NP and SP including p-organics (OA), black carbon (BC), ammonium (NH_4), sulphate (SO_4) and nitrate (NO_3), based on mass concentrations.

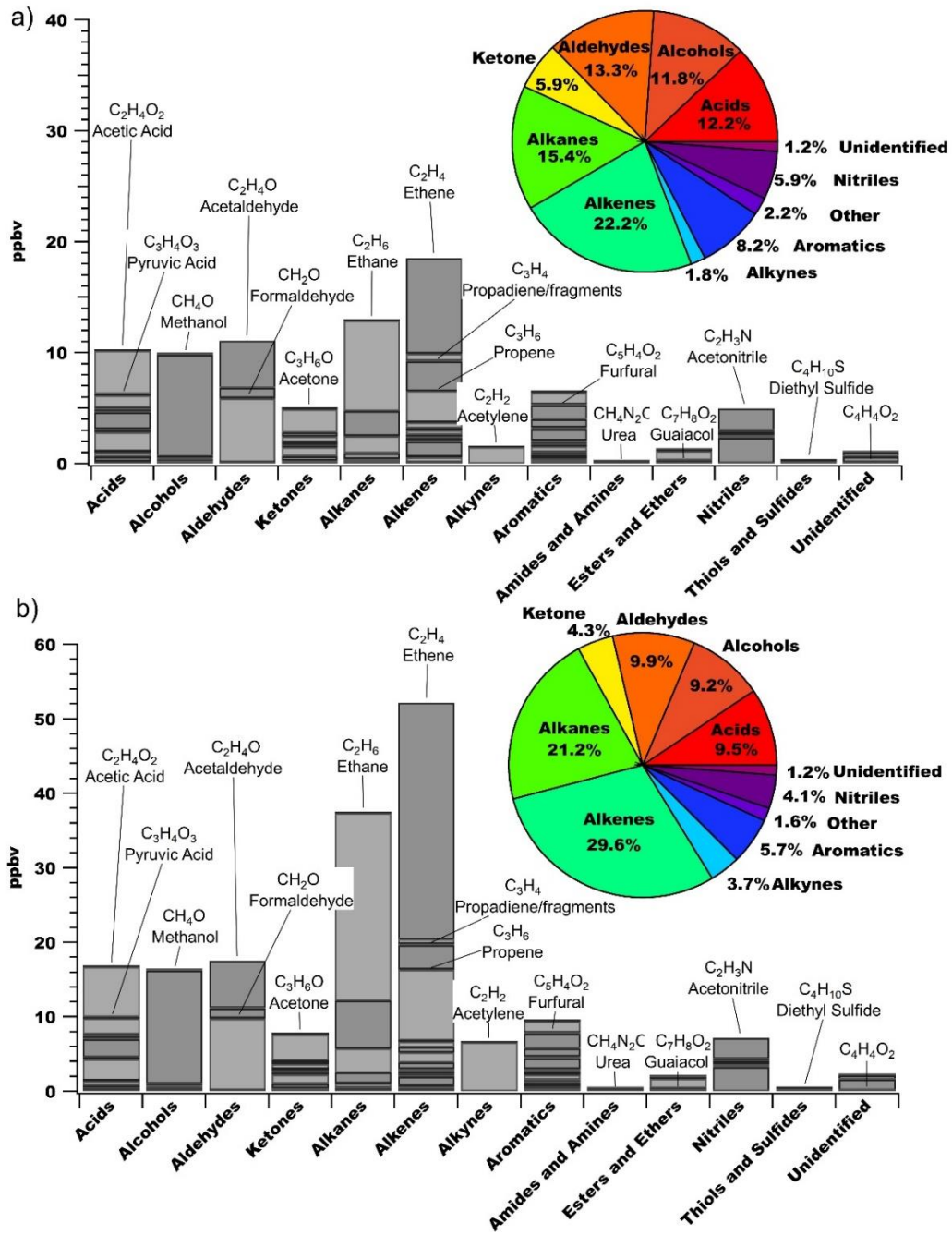

Figure S5. Background-subtracted mixing ratios of individually measured NMOGs from the PTRMS, CIMS and AWAS are shown for thirteen chemical classes for the a) NP and b) SP. In some cases, compounds are double- (or triple-) counted if they can be identified in more than one category. For example, phenol is an alcohol + an aromatic; guaiacol is an alcohol + an ether + an aromatic. In the pie chart, the *Other* category includes amides, amines, ethers, thiols and sulfides. The *Unidentified* category contains molecular formulas detected but the compound(s) could not be identified.

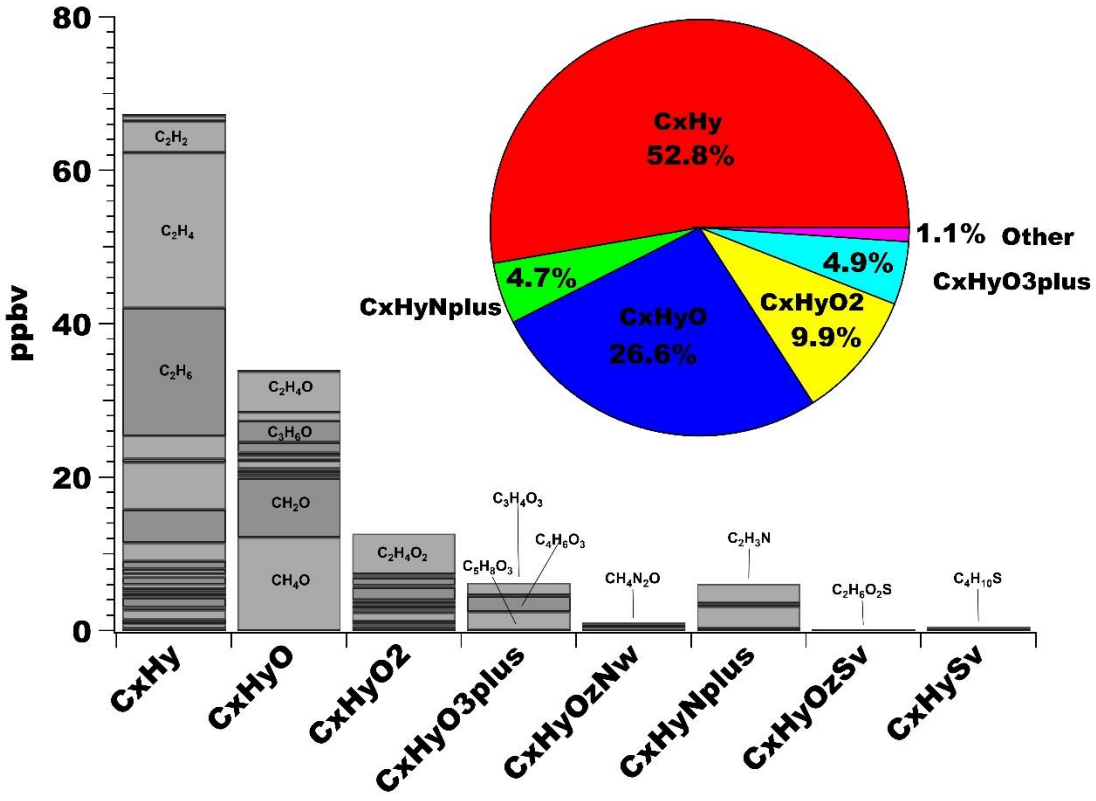

443

444 Figure S6. Background-subtracted average mixing ratios of individually measured NMOGs from the
445 PTRMS, CIMS and AWAS are shown for molecular formulae classes. The *Unidentified* category
446 contains molecular formulas detected but the compound(s) could not be identified.

447

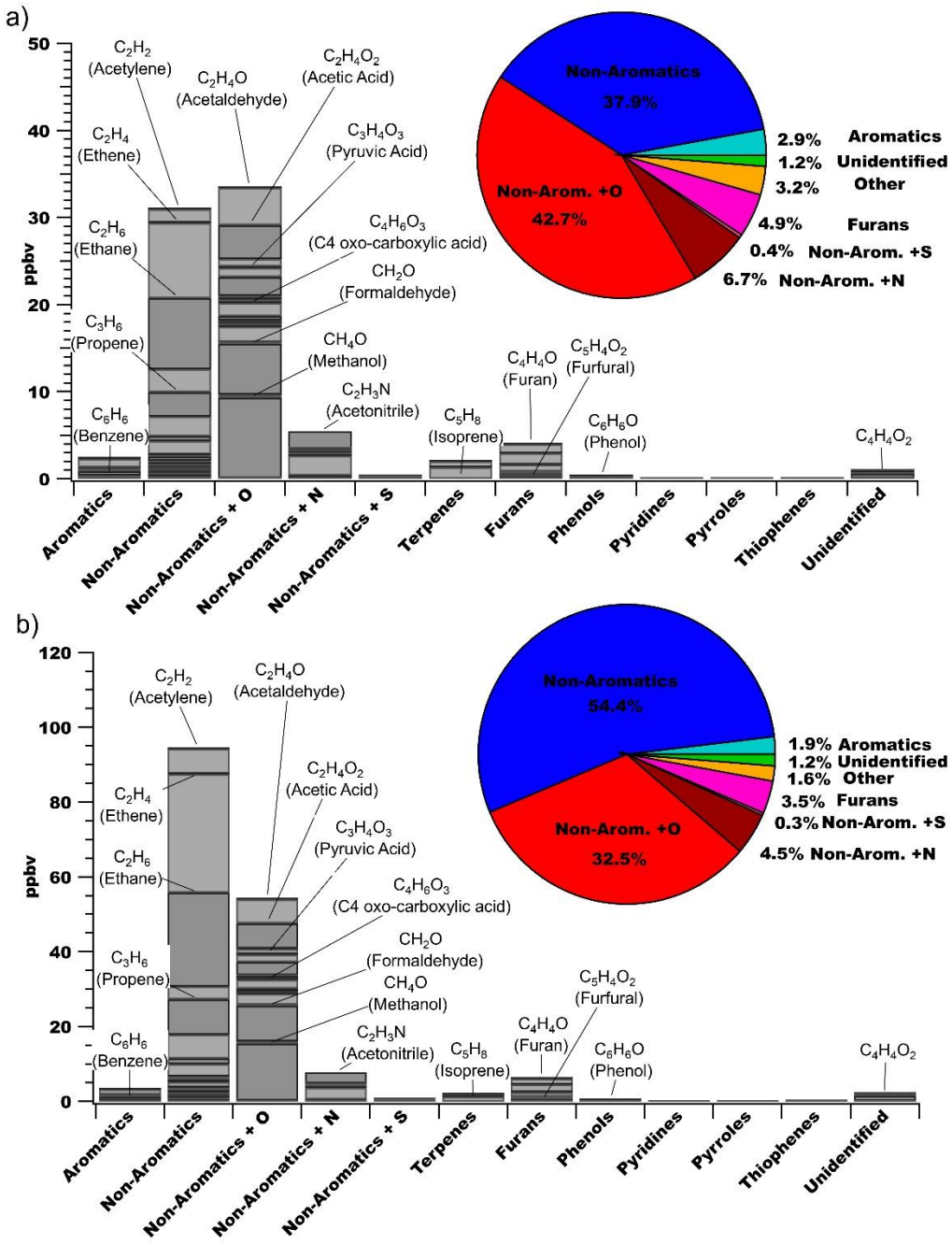

Figure S7. Average mixing ratios of individually measured NMOGs from the PTRMS, CIMS and AWAS by structural group for the a) NP and b) SP. The *Other* category is the sum of terpenes, phenols, pyridines, pyrroles and thiophenes.

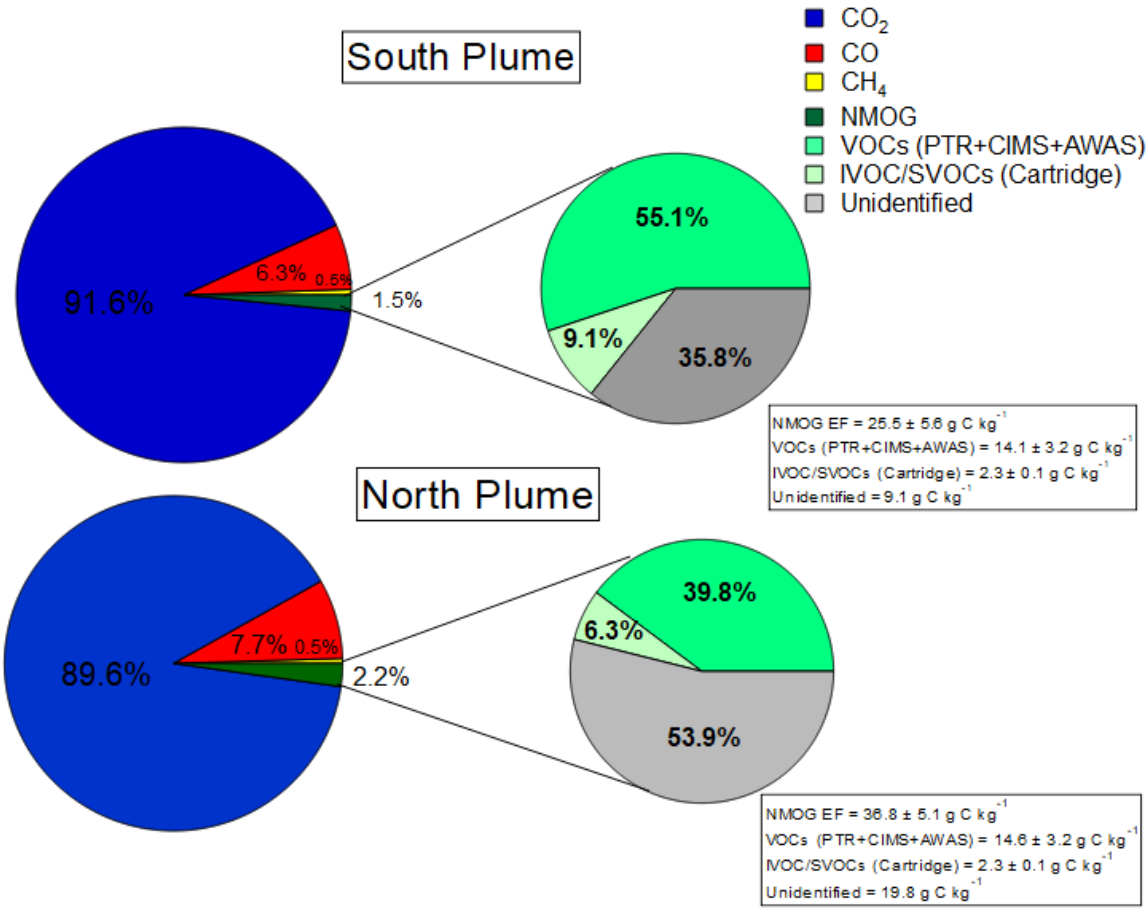

Figure S8. Percent contributions of carbon-containing compounds to the TC based on EFs (in terms of carbon fraction) for the SP and NP. Pie charts on the right show the percent breakdown of the measured NMOGs and the remaining unidentified portion. Note, the I/SVOC measurements represent the integrated average encompassing both plumes.

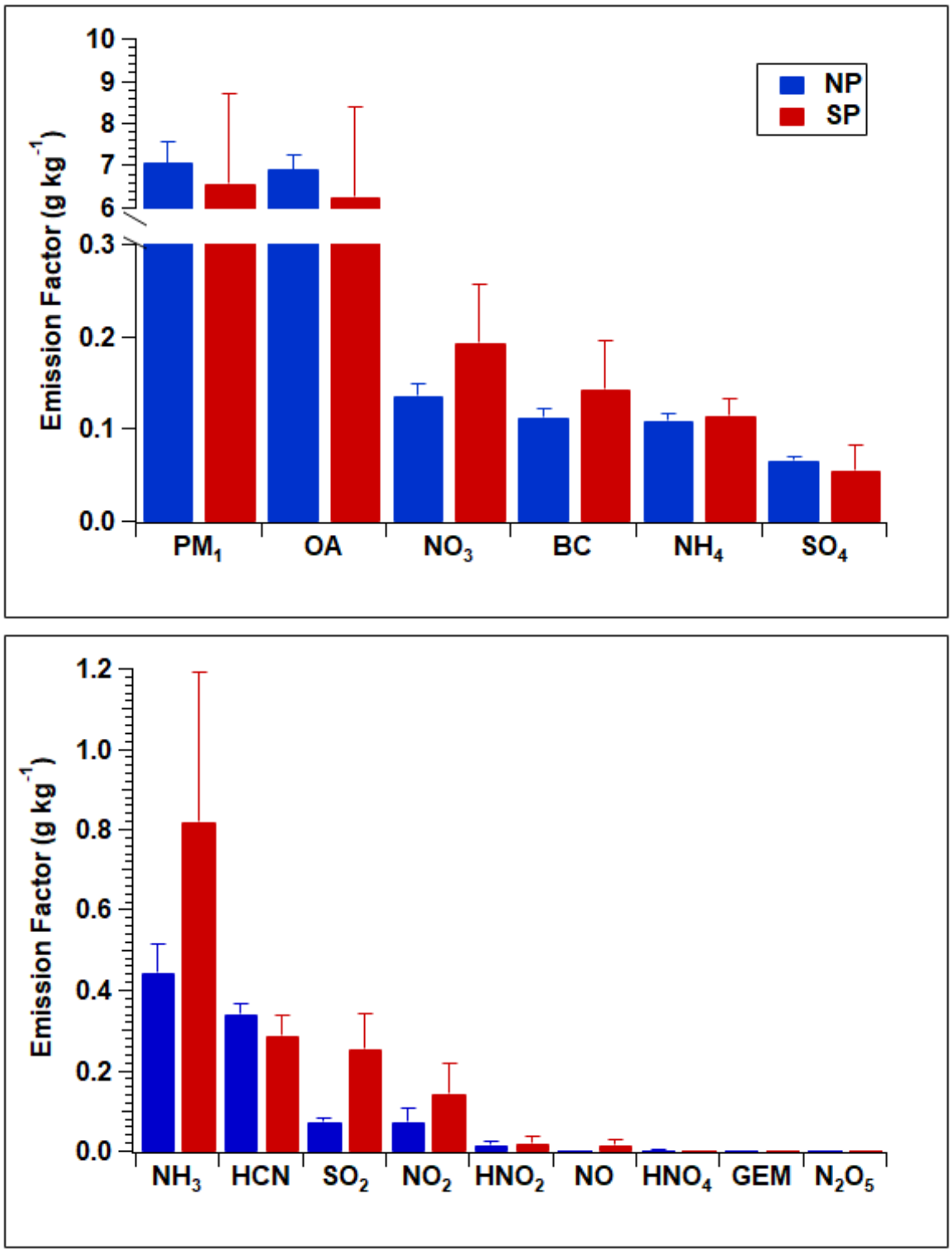

Figure S9. Emission factors (EF) (g kg^{-1}) for the SP and NP determined from measurements of a) particle species; and b) inorganic gas-phase species.

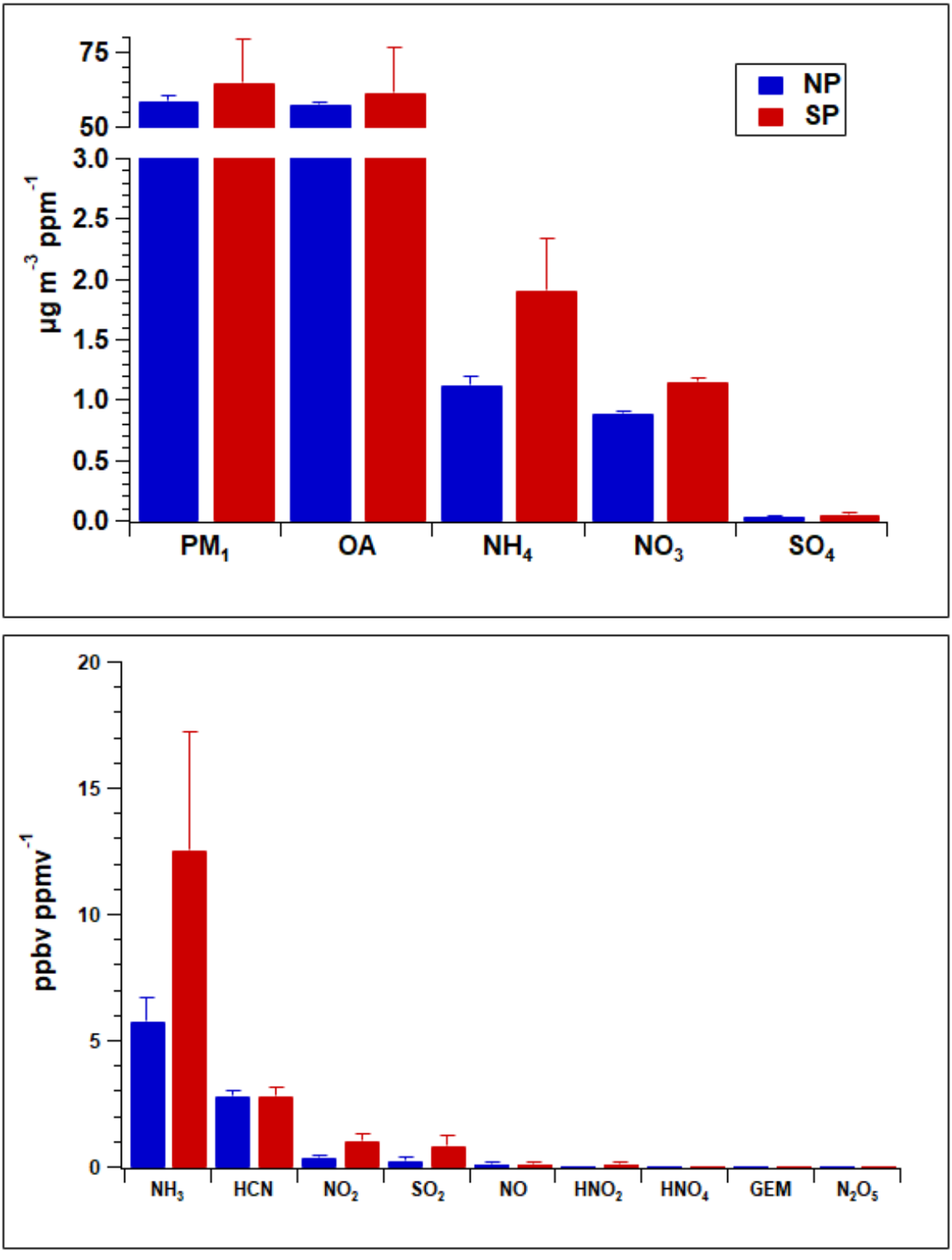

Figure S10. Emission ratios (ER) for the SP and NP determined from measurements of a) particle species (µg m^{-3} ppm^{-1}); and b) inorganic gas-phase species (ppb ppm^{-1}).

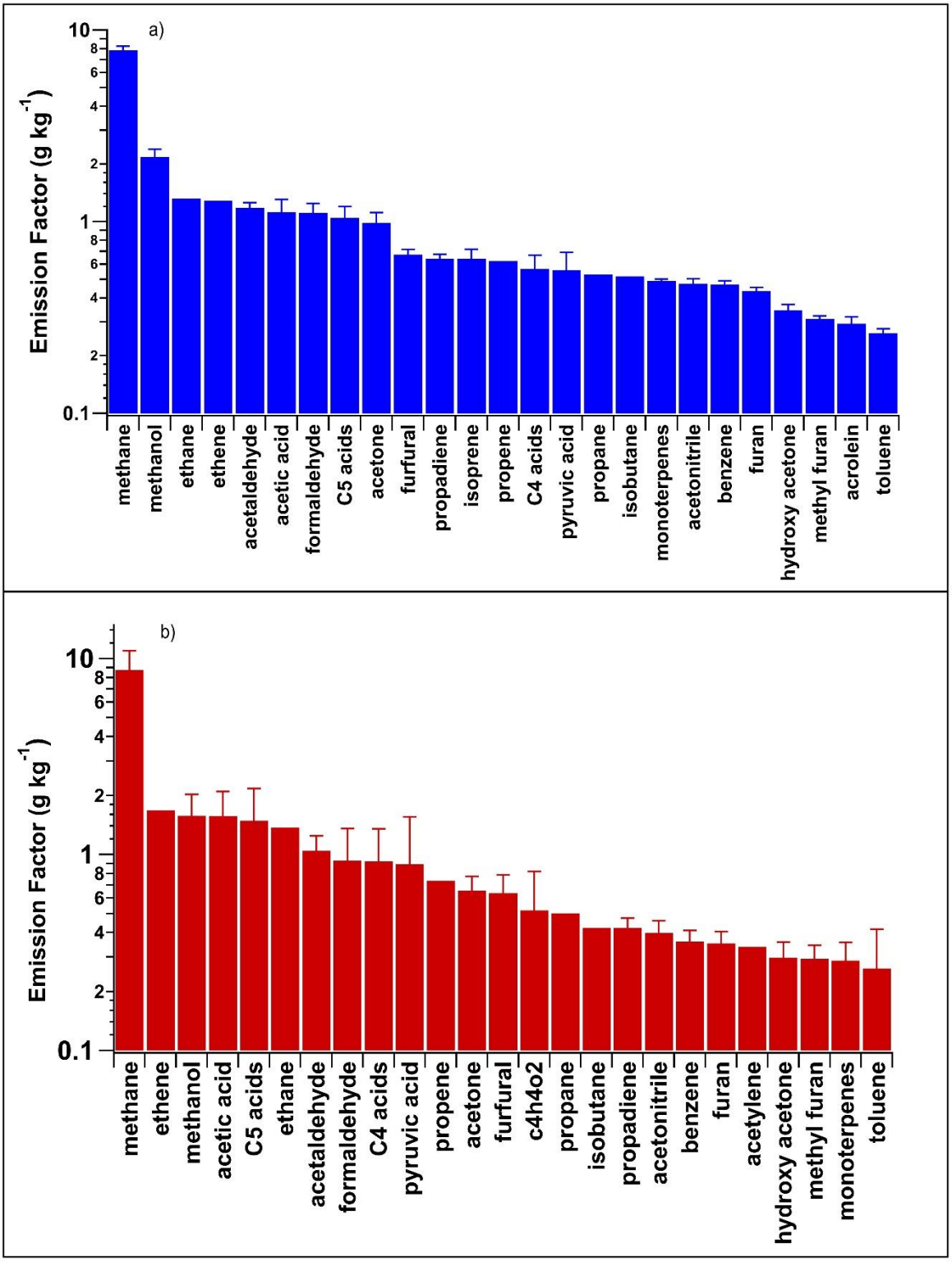

Figure S11. Emission factors (EF) (g kg^{-1}) for the a) NP and b) SP for the top 25 measured gas-phase organic species. C5 acids = C5 oxo-carboxylic acids, C4 acids = C4 oxo-carboxylic acids, propadiene = fragments/propadiene, hydroxy acetone = hydroxy acetone/ ethyl formate.

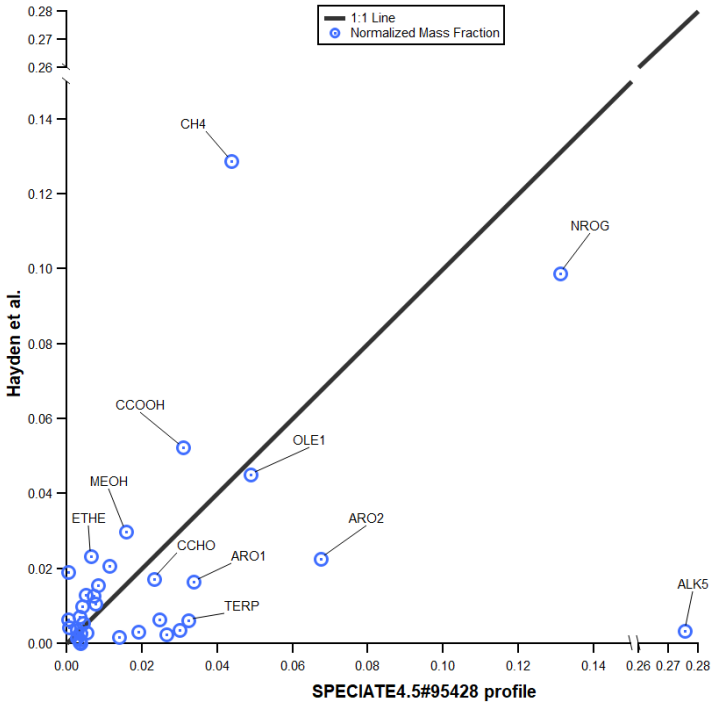

Figure S12. Comparison of the organic gas speciation profile determined from this study (Hayden et al.) with that used by the SAPRC-11 mechanism (SPECIATE4.5#95428). EFs in the present study were mapped to the SAPRC-11 model mechanism species and normalized to the $NMOG_T$ (which includes the unidentified mass fraction), to create the total organic gas mass speciation profile. The normalized model species fraction is plotted against similarly treated mass speciation profile from the EPA SPECIATEv4.5 #95428 for wildfire smoldering emissions. Note that for comparison purposes the non-standard SAPRC-11 species in the present study are lumped, such that SESQ is summed with TERP, and IVOC, WSOC and NVOL are summed with NROG.

References

Akagi, S. K., Yokelson, R. J., Wiedinmyer, C., Alvarado, M. J., Reid, J. S., Karl, T., Crounse, J. D., and Wennberg, P. O.: Emission factors for open and domestic biomass burning for use in atmospheric models, Atmos. Chem. Phys., 11, 4039-4072, https://doi.org/10.5194/acp-11-4039-2011, 2011.

Allan, J. D., Jimenez, J. L., Williams, P. I., Alfarra, M. R., Bower, K. N., Jayne, J. T., Coe, H., and Worsnop, D. R.: Quantitative sampling using an Aerodyne Aerosol Mass Spectrometer 1. Techniques of data interpretation and error analysis, J. Geophys. Res.-Atmos, 108, 4090, https://doi.org/10.1029/2002JD002358, 2003.

Andreae, M. O. and Merlet, P.: Emission of trace gases and aerosols from biomass burning, Global Biogeochem. Cy., 15, 955-966, https://doi.org/10.1029/2000GB001382, 2001.

Baray, S., Darlington, A., Gordon, M., Hayden, K. L., Leithead, A., Li, S. M., Liu, P. S. K., Mittermeier, R. L., Moussa, S. G., O'Brien, J., Staebler, R., Wolde, M., Worthy, D., and McLaren, R.: Quantification of methane sources in the Athabasca Oil Sands Region of Alberta by aircraft mass balance, Atmos. Chem. Phys., 18, 7361-7378, https://doi.org/10.5194/acp-18-7361-2018, 2018.

Baumgardner, D., Kok, G., and Raga, G.: Warming of the Arctic lower stratosphere by light absorbing particles, Geophys. Res. Lett., 31, L06117, https://doi.org/10.1029/2003GL018883, 2004.

Bertschi, I., Yokelson, R. J., Ward, D. E., Babbitt, R. E., Susott, R. A., Goode, J. G., and Hao, W. M.: Trace gas and particle emissions from fires in large diameter and belowground biomass fuels, J. Geophys. Res.-Atmos, 108, 8472, https://doi.org/10.1029/2002JD002100, 2003.

Cai, Y., Montague, D. C., Mooiweer-Bryan, W., and Deshler, T.: Performance characteristics of the ultra high sensitivity aerosol spectrometer for particles between 55 and 800nm: Laboratory and field studies, J. Aerosol Sci., 39, 759-769, https://doi.org/10.1016/j.jaerosci.2008.04.007, 2008.

Clyne, M. A. A., Thrush, B. A., and Wayne, R. P.: Kinetics of the chemiluminescent reaction between nitric oxide and ozone, Trans. Faraday Soc., 60, 359-370, https://doi.org/10.1039/TF9646000359, 1964.

Cole, A. S., Steffen, A., Eckley, C. S., Narayan, J., Pilote, M., Tordon, R., Graydon, J. A., St. Louis, V. L., Xu, X., and Branfireun, B. A.: A survey of mercury in air and precipitation across Canada: Patterns and trends, Atmosphere, 5, 635-668, https://doi.org/10.3390/atmos5030635, 2014.

DeCarlo, P. F., Dunlea, E. J., Kimmel, J. R., Aiken, A. C., Sueper, D., Crounse, J., Wennberg, P. O., Emmons, L., Shinozuka, Y., Clarke, A., Zhou, J., Tomlinson, J., Collins, D. R., Knapp, D., Weinheimer, A. J., Montzka, D. D., Campos, T., and Jimenez, J. L.: Fast airborne aerosol size and chemistry measurements above Mexico City and Central Mexico during the MILAGRO campaign, Atmos. Chem. Phys., 8, 4027-4048, https://doi.org/10.5194/acp-8-4027-2008, 2008.

Ditto, J. C., He, M., Hass-Mitchell, T. N., Moussa, S. G., Hayden, K., Li, S. M., Liggio, J., Leithead, A., Lee, P., Wheeler, M. J., Wentzell, J. J. B., and Gentner, D. R.: Atmospheric evolution of emissions from a boreal forest fire: the formation of highly functionalized oxygen-, nitrogen-, and sulfur-containing organic compounds, Atmos. Chem. Phys., 21, 255-267, https://doi.org/10.5194/acp-21-255-2021, 2021.

Drewnick, F., Schwab, J. J., Jayne, J. T., Canagaratna, M., Worsnop, D. R., and Demerjian, K. L.: Measurement of ambient aerosol composition during the PMTACS-NY 2001 using an aerosol mass spectrometer. Part I: Mass concentrations special issue of aerosol science and technology on findings

from the Fine Particulate Matter Supersites Program, Aerosol Sci. Tech., 38, 92-103, https://doi.org/10.1080/02786820390229507, 2004.

Dunlea, E. J., DeCarlo, P. F., Aiken, A. C., Kimmel, J. R., Peltier, R. E., Weber, R. J., Tomlinson, J., Collins, D. R., Shinozuka, Y., McNaughton, C. S., Howell, S. G., Clarke, A. D., Emmons, L. K., Apel, E. C., Pfister, G. G., van Donkelaar, A., Martin, R. V., Millet, D. B., Heald, C. L., and Jimenez, J. L.: Evolution of Asian aerosols during transpacific transport in INTEX-B, Atmos. Chem. Phys., 9, 7257-7287, https://doi.org/10.5194/acp-9-7257-2009, 2009.

Fehsenfeld, F. C., Dickerson, R. R., Hübler, G., Luke, W. T., Nunnermacker, L. J., Williams, E. J., Roberts, J. M., Calvert, J. G., Curran, C. M., Delany, A. C., Eubank, C. S., Fahey, D. W., Fried, A., Gandrud, B. W., Langford, A. O., Murphy, P. C., Norton, R. B., Pickering, K. E., and Ridley, B. A.: A ground-based intercomparison of NO, NO_x, and NO_y measurement techniques, J. Geophys. Res.-Atmos, 92, 14710-14722, https://doi.org/10.1029/JD092iD12p14710, 1987.

Hatch, L. E., Yokelson, R. J., Stockwell, C. E., Veres, P. R., Simpson, I. J., Blake, D. R., Orlando, J. J., and Barsanti, K. C.: Multi-instrument comparison and compilation of non-methane organic gas emissions from biomass burning and implications for smoke-derived secondary organic aerosol precursors, Atmos. Chem. Phys., 17, 1471-1489, https://doi.org/10.5194/acp-17-1471-2017, 2017.

Jimenez, J. L., Jayne, J. T., Shi, Q., Kolb, C. E., Worsnop, D. R., Yourshaw, I., Seinfeld, J. H., Flagan, R. C., Zhang, X., Smith, K. A., Morris, J. W., and Davidovits, P.: Ambient aerosol sampling using the Aerodyne Aerosol Mass Spectrometer, J. Geophys. Res.-Atmos, 108, 8425, https://doi.org/10.1029/2001JD001213, 2003.

Khare, P., Marcotte, A., Sheu, R., Walsh, A. N., Ditto, J. C., and Gentner, D. R.: Advances in offline approaches for trace measurements of complex organic compound mixtures via soft ionization and high-resolution tandem mass spectrometry, J. Chromatogr. A, 1598, 163-174, https://doi.org/10.1016/j.chroma.2019.03.037, 2019.

Kleinman, L. I., Springston, S. R., Daum, P. H., Lee, Y. N., Nunnermacker, L. J., Senum, G. I., Wang, J., Weinstein-Lloyd, J., Alexander, M. L., Hubbe, J., Ortega, J., Canagaratna, M. R., and Jayne, J.: The time evolution of aerosol composition over the Mexico City plateau, Atmos. Chem. Phys., 8, 1559-1575, https://doi.org/10.5194/acp-8-1559-2008, 2008.

Koss, A. R., Sekimoto, K., Gilman, J. B., Selimovic, V., Coggon, M. M., Zarzana, K. J., Yuan, B., Lerner, B. M., Brown, S. S., Jimenez, J. L., Krechmer, J., Roberts, J. M., Warneke, C., Yokelson, R. J., and de Gouw, J.: Non-methane organic gas emissions from biomass burning: identification, quantification, and emission factors from PTR-ToF during the FIREX 2016 laboratory experiment, Atmos. Chem. Phys., 18, 3299-3319, https://doi.org/10.5194/acp-18-3299-2018, 2018.

Kupc, A., Williamson, C., Wagner, N. L., Richardson, M., and Brock, C. A.: Modification, calibration, and performance of the Ultra-High Sensitivity Aerosol Spectrometer for particle size distribution and volatility measurements during the Atmospheric Tomography Mission (ATom) airborne campaign, Atmos. Meas. Tech., 11, 369-383, https://doi.org/10.5194/amt-11-369-2018, 2018.

Lee, B. H., Lopez-Hilfiker, F. D., Mohr, C., Kurtén, T., Worsnop, D. R., and Thornton, J. A.: An Iodide-Adduct High-Resolution Time-of-Flight Chemical-Ionization Mass Spectrometer: Application to Atmospheric Inorganic and Organic Compounds, Environmental Science & Technology, 48, 6309-6317, 10.1021/es500362a, 2014.

Lee, B. H., Lopez-Hilfiker, F. D., Veres, P. R., McDuffie, E. E., Fibiger, D. L., Sparks, T. L., Ebben, C. J., Green, J. R., Schroder, J. C., Campuzano-Jost, P., Iyer, S., D'Ambro, E. L., Schobesberger, S., Brown, S. S., Wooldridge, P. J., Cohen, R. C., Fiddler, M. N., Bililign, S., Jimenez, J. L., Kurtén, T., Weinheimer, A. J., Jaegle, L., and Thornton, J. A.: Flight Deployment of a High-Resolution Time-of-Flight Chemical Ionization Mass Spectrometer: Observations of Reactive Halogen and Nitrogen Oxide Species, Journal of Geophysical Research: Atmospheres, 123, 7670-7686, https://doi.org/10.1029/2017JD028082, 2018.

Leifer, I., Melton, C. Tratt, D.M., Buckland, K.N., Clarisse, L., Coheur, P., Frash, J., Gupta, M., Johnson, P.D., Leen, J.B., Van Damme, M., Whitburn, S., and Yurganov, L.: Remote sensing and in situ measurements of methane and ammonia emissions from a megacity dairy complex: Chino, CA, Environ. Poll., 221, 37-51, https://doi.org/10.1016/j.envpol.2016.09.083, 2017.

Lerner, B. M., Gilman, J. B., Aikin, K. C., Atlas, E. L., Goldan, P. D., Graus, M., Hendershot, R., Isaacman-VanWertz, G. A., Koss, A., Kuster, W. C., Lueb, R. A., McLaughlin, R. J., Peischl, J., Sueper, D., Ryerson, T. B., Tokarek, T. W., Warneke, C., Yuan, B., and de Gouw, J. A.: An improved, automated whole air sampler and gas chromatography mass spectrometry analysis system for volatile organic compounds in the atmosphere, Atmos. Meas. Tech., 10, 291-313, https://doi.org/10.5194/amt-10-291-2017, 2017.

Li, S.-M., Leithead, A., Moussa, S. G., Liggio, J., Moran, M. D., Wang, D., Hayden, K., Darlington, A., Gordon, M., Staebler, R., Makar, P. A., Stroud, C. A., McLaren, R., Liu, P. S. K., O'Brien, J., Mittermeier, R. L., Zhang, J., Marson, G., Cober, S. G., Wolde, M., and Wentzell, J. J. B.: Differences between measured and reported volatile organic compound emissions from oil sands facilities in Alberta, Canada, P. Natl. Acad. Sci. USA, 114, E3756-E3765, https://doi.org/10.1073/pnas.1617862114, 2017.

Liggio, J., Stroud, C. A., Wentzell, J. J. B., Zhang, J., Sommers, J., Darlington, A., Liu, P. S. K., Moussa, S. G., Leithead, A., Hayden, K., Mittermeier, R. L., Staebler, R., Wolde, M., and Li, S.-M.: Quantifying the Primary Emissions and Photochemical Formation of Isocyanic Acid Downwind of Oil Sands Operations, Environmental Science & Technology, 51, 14462-14471, 10.1021/acs.est.7b04346, 2017.

McGee, T.K.: Evacuating First Nations during wildfires in Canada, Fire Safety Journ., 120, https://doi.org/10.1016/j.firesaf.2020.103120, 2020.

McLagan, D. S., Stupple, G. W., Darlington, A., Hayden, K., and Steffen, A.: Where there is smoke there is mercury: Assessing boreal forest fire mercury emissions using aircraft and highlighting uncertainties associated with upscaling emissions estimates, Atmos. Chem. Phys., 21, 5635-5653, https://doi.org/10.5194/acp-21-5635-2021, 2021.

Middlebrook, A. M., Bahreini, R., Jimenez, J. L., and Canagaratna, M. R.: Evaluation of composition-dependent collection efficiencies for the aerodyne aerosol mass spectrometer using field data, Aerosol Sci. Tech., 46, 258-271, https://doi.org/10.1080/02786826.2011.620041, 2012.

Mungall, E. L., Abbatt, J. P. D., Wentzell, J. J. B., Lee, A. K. Y., Thomas, J. L., Blais, M., Gosselin, M., Miller, L. A., Papakyriakou, T., Willis, M. D., and Liggio, J.: Microlayer source of oxygenated volatile organic compounds in the summertime marine Arctic boundary layer, Proceedings of the National Academy of Sciences of the United States of America, 114, 6203-6208, 10.1073/pnas.1620571114, 2017.

Neuman, J. A., Huey, L. G., Ryerson, T. B., and Fahey, D. W.: Study of Inlet Materials for Sampling Atmospheric Nitric Acid, Environmental Science & Technology, 33, 1133-1136, 10.1021/es980767f, 1999.

Penkett, S., Gilge, S., Plass-Duelmer, C., Galbally, I., Brough, N., Bottenheim, J., Flocke, F., Gerwig, H., Lee, J., Milton, M., Rohrer, F., Ryerson, T., Steinbacher, M., Torseth, K., and Wielgosz, R.: WMO/GAW

expert workshop on global long-term measurements of nitrogen oxides and recommendations for GAW nitrogen oxides network, World Meteorological Organization, Hohenpeissenberg, Germany, 2011.

Permar, W., Wang, Q., Selimovic, V., Wielgasz, C., Yokelson, R. J., Hornbrook, R. S., Hills, A. J., Apel, E. C., Ku, I.-T., Zhou, Y., Sive, B. C., Sullivan, A. P., Collett Jr, J. L., Campos, T. L., Palm, B. B., Peng, Q., Thornton, J. A., Garofalo, L. A., Farmer, D. K., Kreidenweis, S. M., Levin, E. J. T., DeMott, P. J., Flocke, F., Fischer, E. V., and Hu, L.: Emissions of trace organic gases from western U.S. wildfires based on WE-CAN aircraft measurements, J. Geophys. Res.-Atmos, 126, e2020JD033838, https://doi.org/10.1029/2020JD033838, 2021.

Quinn, P. K., Bates, T. S., Coffman, D., Onasch, T. B., Worsnop, D., Baynard, T., de Gouw, J. A., Goldan, P. D., Kuster, W. C., Williams, E., Roberts, J. M., Lerner, B., Stohl, A., Pettersson, A., and Lovejoy, E. R.: Impacts of sources and aging on submicrometer aerosol properties in the marine boundary layer across the Gulf of Maine, J. Geophys. Res.-Atmos, 111, D23S36, https://doi.org/10.1029/2006JD007582, 2006.

Ridley, B. A. and Grahek, F. E.: A small, low flow, high sensitivity reaction vessel for NO chemiluminescence detectors, J. Atmos. Ocean. Tech., 7, 307-311, https://doi.org/10.1175/1520-0426(1990)007<0307:Aslfhs>2.0.Co;2, 1990.

Roberts, J. M., Veres, P., Warneke, C., Neuman, J. A., Washenfelder, R. A., Brown, S. S., Baasandorj, M., Burkholder, J. B., Burling, I. R., Johnson, T. J., Yokelson, R. J., and De Gouw, J.: Measurement of HONO, HNCO, and other inorganic acids by negative-ion proton-transfer chemical-ionization mass spectrometry (NI-PT-CIMS): Application to biomass burning emissions, Atmospheric Measurement Techniques, 3, 981-990, 10.5194/amt-3-981-2010.

Schwarz, J. P., Gao, R. S., Fahey, D. W., Thomson, D. S., Watts, L. A., Wilson, J. C., Reeves, J. M., Darbeheshti, M., Baumgardner, D. G., Kok, G. L., Chung, S. H., Schulz, M., Hendricks, J., Lauer, A., Kärcher, B., Slowik, J. G., Rosenlof, K. H., Thompson, T. L., Langford, A. O., Loewenstein, M., and Aikin, K. C.: Single-particle measurements of midlatitude black carbon and light-scattering aerosols from the boundary layer to the lower stratosphere, J. Geophys. Res.-Atmos, 111, D16207, https://doi.org/10.1029/2006JD007076, 2006.

Sekimoto, K., Li, S.-M., Yuan, B., Koss, A., Coggon, M., Warneke, C., and de Gouw, J.: Calculation of the sensitivity of proton-transfer-reaction mass spectrometry (PTR-MS) for organic trace gases using molecular properties, Int. J. Mass Spectrom., 421, 71-94, https://doi.org/10.1016/j.ijms.2017.04.006, 2017.

Selimovic, V., Yokelson, R. J., McMeeking, G. R., and Coefield, S.: In situ measurements of trace gases, PM, and aerosol optical properties during the 2017 NW US wildfire smoke event, Atmos. Chem. Phys., 19, 3905-3926, https://doi.org/10.5194/acp-19-3905-2019, 2019.

Sheu, R., Marcotte, A., Khare, P., Charan, S., Ditto, J. C., and Gentner, D. R.: Advances in offline approaches for chemically speciated measurements of trace gas-phase organic compounds via adsorbent tubes in an integrated sampling-to-analysis system, J. Chromatogr. A, 1575, 80-90, https://doi.org/10.1016/j.chroma.2018.09.014, 2018.

Stecher III, H. A., Luther III, G. W., MacTaggart, D. L., Farwell, S. O., Crosley, D. R., Dorko, W. D., Goldan, P. D., Beltz, N., Krischke, U., Luke, W. T., Thornton, D. C., Talbot, R. W., Lefer, B. L., Scheuer, E. M., Benner, R. L., Wu, J., Saltzman, E. S., Gallagher, M. S., and Ferek, R. J.: Results of the Gas-Phase

Sulfur Intercomparison Experiment (GASIE): Overview of experimental setup, results and general conclusions, J. Geophys. Res.-Atmos, 102, 16219-16236, https://doi.org/10.1029/97JD01362, 1997.

Stephens, M., Turner, N., and Sandberg, J.: Particle identification by laser-induced incandescence in a solid-state laser cavity, Appl. Optics, 42, 3726-3736, https://doi.org/10.1364/ao.42.003726, 2003.

Stockwell, C. E., Kupc, A., Witkowski, B., Talukdar, R. K., Liu, Y., Selimovic, V., Zarzana, K. J., Sekimoto, K., Warneke, C., Washenfelder, R. A., Yokelson, R. J., Middlebrook, A. M., and Roberts, J. M.: Characterization of a catalyst-based conversion technique to measure total particulate nitrogen and organic carbon and comparison to a particle mass measurement instrument, Atmos. Meas. Tech., 11, 2749-2768, 10.5194/amt-11-2749-2018, 2018.

Veres, P. R., and Roberts, J. M.: Development of a photochemical source for the production and calibration of acyl peroxynitrate compounds, Atmos. Meas. Tech., 8, 2225-2231, 10.5194/amt-8-2225-2015, 2015.

Veres, P., Roberts, J. M., Burling, I. R., Warneke, C., de Gouw, J., and Yokelson, R. J.: Measurements of gas-phase inorganic and organic acids from biomass fires by negative-ion proton-transfer chemical-ionization mass spectrometry, J. Geophys. Res.-Atmos, 115, D23302, https://doi.org/10.1029/2010JD014033, 2010.

Ward, D. E. and Radke, L. F.: Emissions measurements from vegetation fires: A comparative evaluation of methods and results, in: Fire in the Environment: The Ecological, Atmospheric, and Climatic Importance of Vegetation Fires. Dahlem Workshop Reports: Environmental Sciences Research Report 13, edited by: Crutzen, P. J., and Goldammer, J. G., John Wiley & Sons, Chischester, England, 53-76, 1993.

Williams, E. J., Baumann, K., Roberts, J. M., Bertman, S. B., Norton, R. B., Fehsenfeld, F. C., Springston, S. R., Nunnermacker, L. J., Newman, L., Olszyna, K., Meagher, J., Hartsell, B., Edgerton, E., Pearson, J. R., and Rodgers, M. O.: Intercomparison of ground-based NO_y measurement techniques, J. Geophys. Res.-Atmos, 103, 22261-22280, https://doi.org/10.1029/98JD00074, 1998.